AGU PUBLICATIONS

Geochemistry, Geophysics, Geosystems

RESEARCH ARTICLE
10.1002/2014GC005620

Key Points:
- Source and magma mixing processes are evident in continental subduction factory
- The heterogeneous mantle source is generated by source mixing
- Mineral zonings record the magma mixing between heterogeneous mafic melts

Supporting Information:
- 3G Supporting information

Correspondence to:
L.-Q. Dai,
lqdai@ustc.edu.cn

Citation:
Dai, L.-Q., Z.-F. Zhao, Y.-F. Zheng, and J. Zhang (2015), Source and magma mixing processes in continental subduction factory: Geochemical evidence from postcollisional mafic igneous rocks in the Dabie orogen, *Geochem. Geophys. Geosyst.*, *16*, 659–680, doi:10.1002/2014GC005620.

Received 21 OCT 2014
Accepted 9 FEB 2015
Accepted article online 12 FEB 2015
Published online 6 MAR 2015

Source and magma mixing processes in continental subduction factory: Geochemical evidence from postcollisional mafic igneous rocks in the Dabie orogen

Li-Qun Dai[1], Zi-Fu Zhao[1], Yong-Fei Zheng[1], and Juan Zhang[2]

[1]CAS Key Laboratory of Crust-Mantle Materials and Environments, School of Earth and Space Sciences, University of Science and Technology of China, Hefei, China, [2]State key Laboratory of Continental Dynamics, Department of Geology, Northwest University, Xi'an, China

Abstract Postcollisional mafic igneous rocks commonly exhibit petrological and geochemical heterogeneities, but their origin still remains enigmatic. While source mixing is substantial due to the crust-mantle interaction during continental collision, magma mixing is also significant during postcollisional magmatism. The two processes are illustrated by Early Cretaceous mafic igneous rocks in the Dabie orogen. These mafic rocks show arc-like trace element distribution patterns and enriched Sr-Nd-Pb isotope compositions, indicating their origination from enriched mantle sources. They have variable whole-rock $\varepsilon_{Nd}(t)$ values of −17.6 to −5.2 and zircon $\varepsilon_{Hf}(t)$ values of −29.0 to −7.7, pointing to source heterogeneities. Such whole-rock geochemical features are interpreted by the source mixing through melt-peridotite reaction in the continental subduction channel. Clinopyroxene and plagioclase megacrystals show complex textural and compositional variations, recording three stages of mineral crystallization during magma evolution. Cpx-1 core has low Cr and Ni but high Ba, Rb and K, indicating its crystallization from a mafic melt (Melt 1) derived from partial melting of hydrous peridotite rich in phlogopite. Cpx-1 mantle and Cpx-2 exhibit significantly high Cr, Ni and Al_2O_3 but low Rb and Ba, suggesting their crystallization from pyroxenite-derived mafic melt (Melt 2). Whole-rock initial $^{87}Sr/^{86}Sr$ ratios of gabbro lies between those of Pl-1core (crystallized from Melt 1) and Pl-1 mantle and Pl-2 core (crystallized from Melt 2), providing isotopic evidence for magma mixing between Melt 1 and Melt 2. Taken together, a heterogeneously enriched mantle source would be generated by the source mixing due to reaction of the overlying subcontinental lithospheric mantle wedge peridotite with felsic melts derived from partial melting of different rocks of the deeply subducted continental crust during the continental collision. The magma mixing would occur between mafic melts that were derived from partial melting of the heterogeneously metasomatic mantle domains in the postcollisional stage. As a consequence, the source and magma mixing processes in the continental subduction factory are responsible for the significant variations in the whole-rock and mineral geochemistries of postcollisional mafic igneous rocks.

1. Introduction

It is known that interaction of the mantle wedge with fluids derived from dehydration of subducting oceanic crust is responsible for supra-subduction-zone (SSZ) arc volcanism [e.g., *Hawkesworth et al*., 1991; *Tatsumi and Eggins*, 1995; *Spandler and Pirard*, 2013]. This interaction is a process of source mixing between slab-derived fluids and the mantle wedge peridotite, which is a key to recycling of crustal components at oceanic subductuion zones and thus usually referred to part of the subduction factory [e.g., *Stern*, 2002]. As such, the fluid-peridotite reaction at the slab-mantle interface in oceanic subduction channel is responsible for the generation of mantle sources for oceanic arc basalts [*Bebout*, 2007; *Zheng*, 2012]. If felsic melts instead of aqueous fluids would be produced by partial melting of subducted crustal rocks, the melt-peridotite reaction at the slab-mantle interface in subcontinental subduction channel is responsible for the generation of mantle sources for continental arc andesites [*Chen et al*., 2014]. Thus, slab-derived fluids/melts are a critical medium that transfer the crustal components to the mantle sources of oceanic and continental arc volcanics. It is possible that the melt-peridotite reaction would be also operated the slab-mantle

interface during the subduction of continental crust to mantle depths [*Zheng and Hermann*, 2014], generating olivine-poor ultramafic lithologies for mafic magmatism in the continental subduction factory [*Zhao et al*., 2013]. Therefore, the source mixing between the subducted crustal components and the mantle wedge peridotite is a key to the heterogeneity of mantle sources for mafic igneous rocks.

The source heterogeneity can be indicated not only by the geochemistry of mafic igneous rocks, but also by the lithology of their parental rocks. Studies of mantle-derived xenoliths and experimental petrology suggest that pyroxene, hornblende and phlogopite can form by reaction of the mantle wedge peridotite with hydrous felsic melts derived from dehydration melting of subducting crustal rocks [*Yaxley and Green*, 1998; *Rapp et al*., 1999, 2010; *Prouteau et al*., 2001; *Coltorti et al*., 2004; *Berly et al*., 2006]. As such, the melt-peridotite reaction is a physicochemical mechanism for the source mixing of mafic igneous rocks. In addition, magma mixing between two or more melt batches can result in petrological and geochemical heterogeneities of igneous rocks. In order to decipher the petrogenesis of heterogeneous mafic igneous rocks in continental collision orogens, it is also necessary to take into account the magma mixing, which may have played an important role in modifying the composition of mafic melts with reference to that of their mantle sources. In this case, it is intriguing whether there are the both magma mixing and source mixing for the petrogenesis of heterogeneous postcollisional mafic magmatic rocks.

Postcollisional mafic igneous rocks are widespread in the Dabie-Sulu orogenic belt [*Zhao and Zheng*, 2009], providing us with an excellent opportunity to decipher the processes in the continental subduction factory [*Zheng*, 2012]. A number of whole-rock geochemical studies have revealed that these mafic rocks are characterized by arc-like trace element distribution patterns such as the enrichment of large ion lithophile elements (LILE) and light rare earth elements (LREE), but the depletion of high field strength elements (HFSE). They exhibit high initial $^{87}Sr/^{86}Sr$ ratios and negative $\varepsilon_{Nd}(t)$ values, and different O isotope compositions compared to normal mantle values. In addition, their element and isotope compositions display high heterogeneities [e.g., *Dai et al*., 2011; *Zhang et al*., 2013; *Zhao et al*., 2013]. These features were interpreted to indicate incorporation of the deeply subducted continental crust into their mantle source [e.g., *Jahn et al*., 1999; *Fan et al*., 2004; *Wang et al*., 2005; *Zhao et al*., 2005, 2011; *Huang et al*., 2007; *Dai et al*., 2011, 2012]. However, these previous studies were mainly focused on whole-rock geochemistry [e.g., *Jahn et al*., 1999; *Zhao et al*., 2005; *Huang et al*., 2007; *Xu et al*., 2012], which have limited potential to unravel various petrogenetic processes such as source mixing, partial melting, fractional crystallization, magma mixing, crustal contamination and magma degassing. While these six processes may have operated to variable extents in different stages of petrogenesis, one of these processes may be primarily recorded by a given type of geochemical data. In order to track the magma mixing in addition to the source mixing, for instance, it is necessary to acquire detailed mineralogical information such as mineral inclusions, element and isotope zonings.

In this paper, we present a combined study of mineral in situ element and isotope compositions, zircon U-Pb ages and Lu-Hf isotopes, and whole-rock major-trace elements and Sr-Nd-Pb isotopes for postcollisional mafic igneous rocks from the Dabie orogen. The results are interpreted in an integrated way in order to distinguish the magma mixing from the source mixing during mafic magmatism in the continental collision orogen. The compositional variations of whole-rock and minerals are used to indicate the heterogeneity of mantle source and the effect of magma mixing. As a consequence, this study provides insights into physicochemical processes in the subduction factory, in which the source mixing is realized through the melt-peridotite reaction at the slab-mantle interface in the continental subduction channel whereas the magma mixing is established by blending of mafic melts derived from partial melting of the heterogeneous mantle domains.

2. Geological Setting and Samples

The Dabie-Sulu orogens in east-central China (lower right insert in Figure 1) were generated by continent-continent collision in the Triassic [e.g., *Li et al*., 1999; *Zheng et al*., 2003, 2013a]. Findings of coesite and microdiamond in Dabie-Sulu eclogites and gneisses demonstrate that the continental crust was subducted to mantle depths of >100 km to experience ultrahigh-pressure (UHP) metamorphism [*Okay et al*., 1989; *Wang et al*., 1989; *Xu et al*., 1992]. The UHP metamorphic rocks are prominent in the Dabie orogen and they are mainly composed of granitic orthogneiss, with subordinate eclogite, granulite, amphibolite, marble and migmatite. A number of zircon U-Pb geochronological and mineral O isotope studies demonstrate that the subducted continental crust are primarily composed of Precambrian basement and its sedimentary cover of

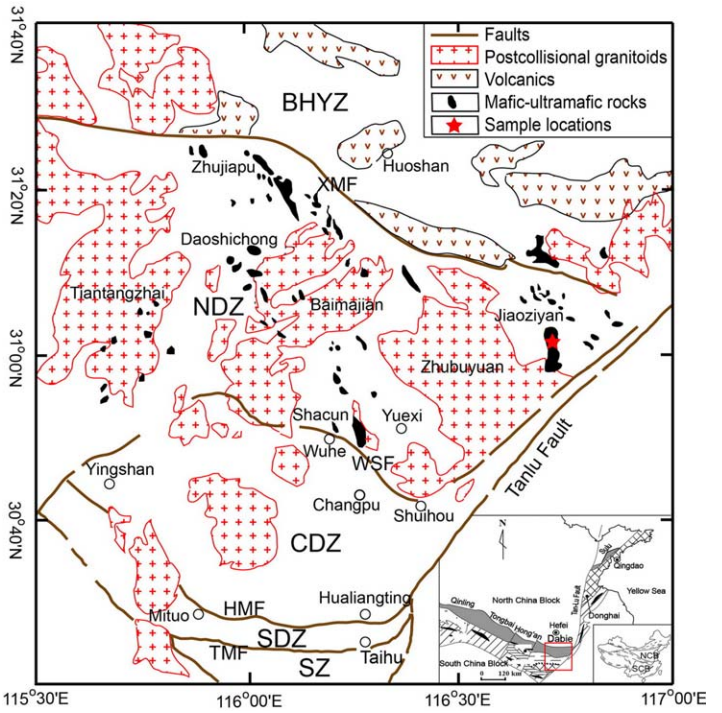

Figure 1. Distributions of postcollisional magmatic rocks in the Dabie orogen [modified after *Liu and Li*, 2008; *Dai et al*., 2011]. Abbreviations: BHYZ = Beihuaiyang low-T/low-P greenschist-facies zone, NDZ = North Dabie high-T/UHP granulite-facies zone, CDZ = Central Dabie mid-T/UHP eclogite-facies zone, SDZ = South Dabie low-T/UHP eclogite-facies zone, SZ = Susong low-T/HP blueschist-facies zone.

the South China Block [e.g., *Zheng et al*., 2003, 2005]. According to metamorphic P-T conditions on the outcrop scale, the Dabie orogen can be subdivided into five major lithotectonic units from north to south (Figure 1): (1) Beihuaiyang low-T/low-P greenschist-facies zone, (2) North Dabie high-T/UHP granulite-facies zone, (3) Central Dabie mid-T/UHP eclogite-facies zone, (4) South Dabie low-T/UHP eclogite-facies zone, and (5) Susong low-T/HP blueschist-facies zone. All of these metamorphic units were extensively intruded by postcollisional igneous rocks of Early Cretaceous [*Zhao and Zheng*, 2009].

Postcollisional magmatism in the Dabie orogen is dominated by voluminous granitoids with minor mafic to ultramafic intrusive and volcanic rocks [*Ma et al*., 1998; *Jahn et al*., 1999; *Chen et al*., 2002; *Zhang et al*., 2002; *Bryant et al*., 2004; *Wang et al*., 2005; *Zhao et al*., 2005, 2007; *Huang et al*., 2007; *Xu et al*., 2012]. Previous studies have demonstrated that these magmatic rocks were primarily emplaced in the Early Cretaceous (113–143 Ma) [*Zhao and Zheng*, 2009]. The mafic-ultramafic intrusive rocks mainly occur in the North Dabie zone, with dominant rock types of gabbro, pyroxenite and hornblendite. They are generally undeformed and exhibit distinct intrusive relations to country-rock gneisses.

Samples used in this study were collected from the Jiaoziyan area in North Dabie (Figure 1). The Jiaoziyan mafic intrusion is one of the biggest mafic-ultramafic intrusions (~30 km^2 in area) in the Dabie orogen. According to petrographic observations and major element analysis, the Jiaoziyan pluton can be divided into gabbro and gabbroic diorite. Some gabbro enclaves can be observed in gabbroic diorite, and they contact the host gabbroic diorite sharply or gradually at various locations (Figure 2a). The gabbro accounts for ~80 % exposure of the pluton and is mainly composed of plagioclase (50–60%), clinopyroxene (15–20%), hornblende (10–15%) and biotite (10–15%), with accessory magnetite, apatite and zircon. Compared to the gabbro, the gabbroic diorite contains relatively more plagioclase (60–65%), hornblende (20–25%), biotite (~20%), but less clinopyroxene (~5%). Most of the rock-forming minerals in the Jiaoziyan mafic intrusion are in the size range of 100–300 μm. Especially, some large clinopyroxene and rare orthopyroxene megacrystals can be observed in some gabbro samples (Figures 2b–2f). Generally, the large clinopyroxene megacrystals can be divided into two groups. Group I clinopyroxene megacrystals (hereafter Cpx-1) exhibit clear zoning with core-mantle-rim structures (up to 3 mm; Figure 2b). Amphibole (hereafter Amp-1) and minor plagioclase occur in clinopyroxene core. Group II clinopyroxene megacrystals (hereafter Cpx-2) are subhedral without clear zoning (Figures 2c–2e), and they are often replaced by amphibole (hereafter Amp-2) at the rim. The boundary between clinopyroxene and amphibole is inter-fingering. Plagioclase inclusion can be observed in Amp-2 (Figures 2c and 2d). The plagioclase megacrystals also can be divided into two groups. Group I plagioclase megacrystals (hereafter Pl-1) exhibit clear zoning with core-mantle-rim structures (Figure 2g). Clinopyroxene, biotite, plagioclase and magnetite inclusions can be observed in the Pl-1 core. There are minor biotite and plagioclase inclusions in the Pl-1 rim. Group II plagioclase megacrystals

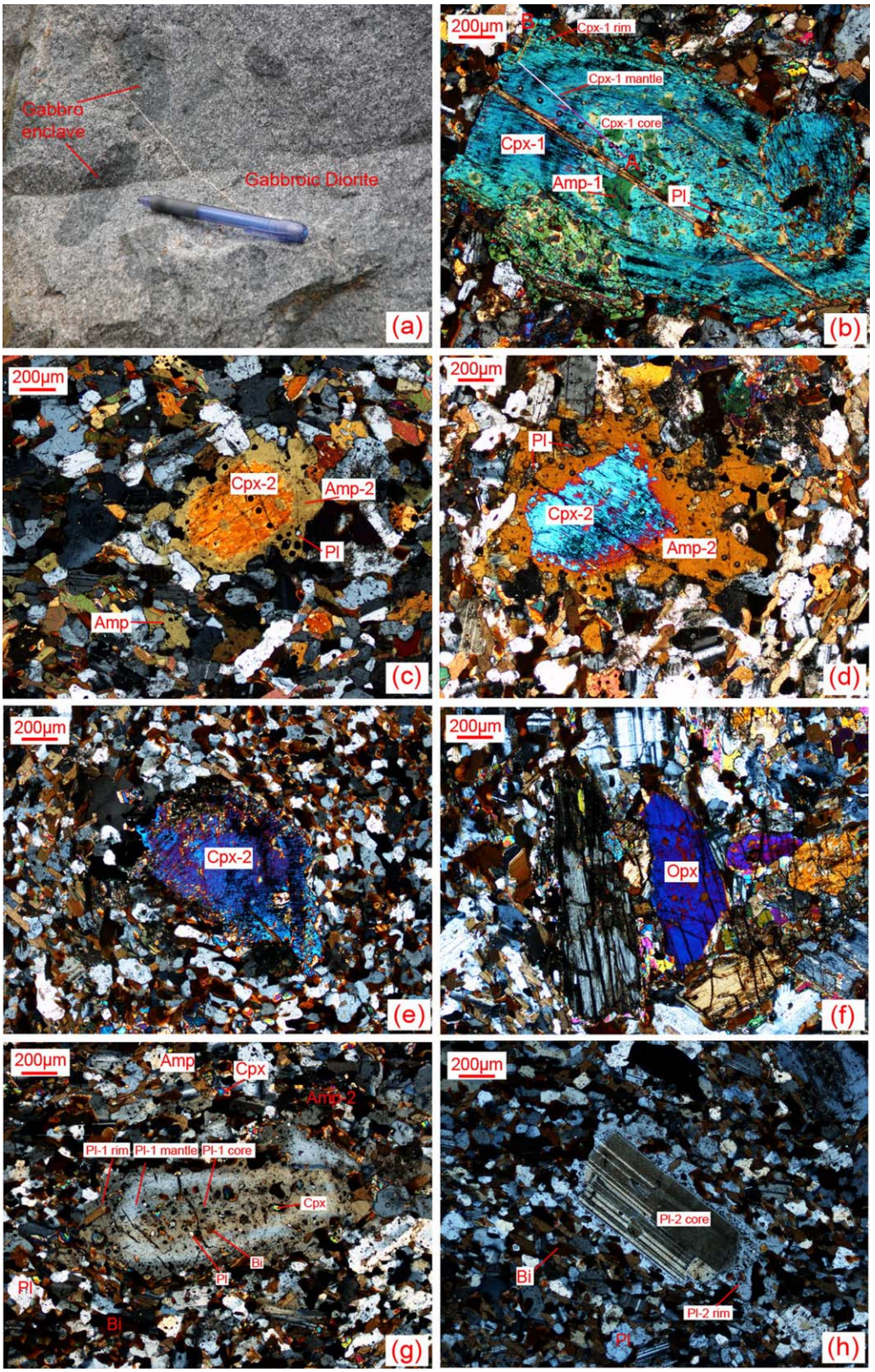

Figure 2. Photographs of characteristic textures for the Jiaoziyan mafic rocks in the Dabie orogen. (a) Gabbro enclaves enclosed in gabbroic diorite, displaying magma mixing at different locations; (b) large clinopyroxene phenocryst with clear zoning with core-mantle-rim structure; (c and d) unzoned clinopyroxene phenocrysts replaced by amphibole at the rim; (e) unzoned clinopyroxene phenocryst; (f) orthopyroxene phenocryst. Abbreviations: Opx-orthopyroxene, Cpx-clinopyroxene, Amphibole-Amp, Bi-biotite, Pl-plagioclase.

(hereafter Pl-2) display clearly core-rim structures (Figure 2h), and the boundary between core and rim is relatively sharp. Plagioclase and minor biotite occur in the Pl-2 rim. Petrographic observations suggest that the orthopyroxene megacrystals do not exhibit significant zoning (Figure 2f).

3. Analytical Methods

Whole-rock major-trace elements and Sr-Nd-Pb isotopes, zircon U-Pb ages and Lu-Hf isotopes, as well as mineral in-situ major-trace elements and Sr isotope compositions were analyzed for the selected Jiaoziyan mafic igneous rocks. Full details of analytical methods are provided in supporting information.

4. Results

4.1. Zircon U-Pb Ages

Gabbro 09JZY14 and gabbroic diorites 09JZY05, 09JZY07 and 09JZY18 were selected for the LA-ICPMS zircon U-Pb dating. The zircon U-Pb isotopic data are presented in supporting information Table S1.

As illustrated in Figure 3, zircon grains are generally euhedral to semi-euhedral, and have grain sizes of 200–400 μm. Most zircon grains exhibit significant oscillatory zoning, indicating magmatic origin. Zircon U-Pb

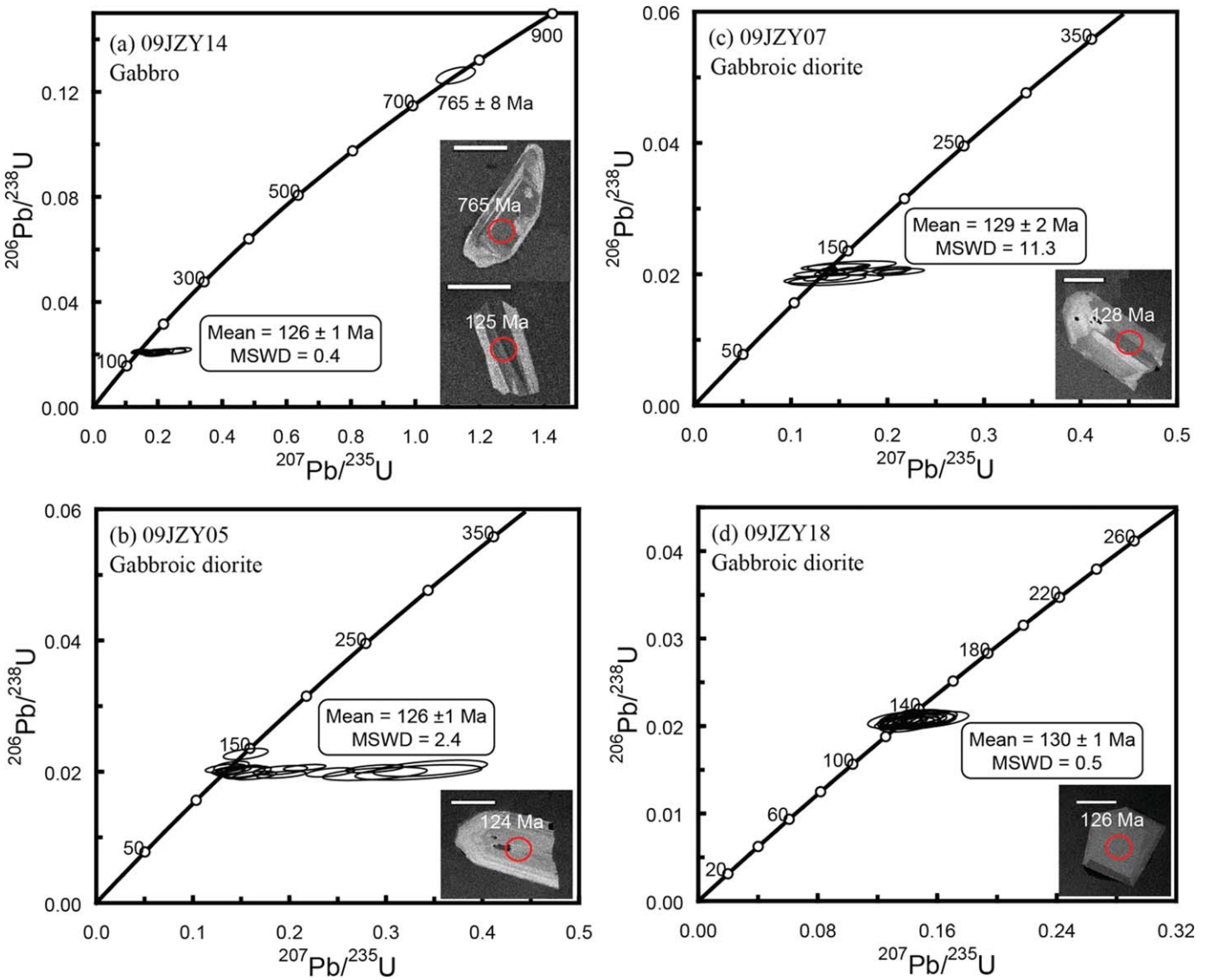

Figure 3. Concordia diagrams of zircon U-Pb isotope data analyzed by the LA-ICPMS technique for the Jiaoziyan mafic rocks in the Dabie orogen. Representative zircon CL images are also shown in the diagrams.

isotope data for the four samples are concordant within analytical errors. Seventeen analyses yield a weighted $^{206}Pb/^{238}U$ age of 126 ± 1 Ma (MSWD = 0.4) for sample 09JZY14, with one concordant U-Pb age of 765 ± 8 Ma for a relict zircon core (Figure 3a). Eighteen analyses also give a weighted $^{206}Pb/^{238}U$ age of 126 ± 1 Ma (MSWD = 2.4) for sample 09JZY05 (Figure 3b). For sample 09ZJP07 (Figure 3c), eighteen analyses yield a weighted $^{206}Pb/^{238}U$ age of 129 ± 2 Ma (MSWD = 11.3). Nineteen analyses for sample 09JZY18 (Figure 3d) give a weighted $^{206}Pb/^{238}U$ age of 130 ± 1 Ma (MSWD = 0.5).

4.2. Whole-Rock Major and Trace Elements

The whole-rock major and trace element data for 15 samples from the Jiaoziyan mafic intrusion are presented in Table 1. In the following discussion, all the major oxides used in diagrams are normalized to volatile-free before plotting. Most of the samples belong to alkaline series on the total alkalis versus SiO_2 diagram (supporting information Figure S1).

The gabbros exhibit relatively restricted SiO_2 contents of 45.68–48.86 wt.%, high Na_2O and K_2O contents ranging from 2.66 to 4.31 wt.% and 0.87 to 2.95 wt.%, respectively (Table 1). They have MgO contents of 3.57–6.96 wt.% with Mg# values of 42.7–59.5 [Mg# = $100\times MgO/(MgO + 0.9\times Fe_2O_3)$]. Most of the gabbroic diorites are also alkalic, with high contents of Na_2O (2.66–4.22 wt.%) and K_2O (1.18–4.90 wt.%). They have relatively high SiO_2 contents of 50.53–53.93 wt.% but variable MgO contents (3.1–6.42 wt.%, Mg# = 45–70.3). On the chondrite-normalized REE diagram (Figure 4a), the gabbros exhibit LREE enrichment with $(La/Yb)_N$ = 10–43.1, and without obvious Eu anomalies (Eu/Eu* = 0.87–1.16). The gabbroic diorites are also characterized by enrichment of LREE, with $(La/Yb)_N$ ratios of 22.2–27.2, and slightly negative Eu anomalies (Eu/Eu* = 0.75–0.96). On the primitive mantle-normalized trace element spidergram (Figure 4b), the gabbros are characterized by enrichment of LILE (Rb and Ba) but depletion of Th, U and HFSE (Nb, Ta, Zr, Hf and Ti). Compared to the gabbros (Th = 0.54–2.66 ppm, U = 0.11–0.45 ppm, Pb = 3.03–9 ppm), the gabbroic diorites have high contents of Th (4.61–11.1 ppm), U (0.71–2.5 ppm), and Pb (9.11–17.3 ppm) (Table 1 and Figure 4b)

4.3. Whole-Rock Sr-Nd-Pb Isotopes

Whole-rock Sr-Nd and Pb isotope compositions are presented in supporting information Tables S2 and S3, respectively. The gabbros have high initial $^{87}Sr/^{86}Sr$ ratios of 0.7066–0.7078 and negative $\varepsilon_{Nd}(t)$ values of −10.1 to −17.6. The gabbroic diorites exhibit similar initial $^{87}Sr/^{86}Sr$ ratios of 0.7072–0.7077 and negative $\varepsilon_{Nd}(t)$ values of −5.2 to −16.2. The initial Pb isotope ratios of gabbros are 16.121–16.606 for $^{206}Pb/^{204}Pb$, 15.273–15.354 for $^{207}Pb/^{204}Pb$ and 36.753–37.232 for $^{208}Pb/^{204}Pb$. The gabbroic diorites have similar initial Pb isotope ratios, with 16.154–16.405 for $^{206}Pb/^{204}Pb$, 15.307–15.524 for $^{207}Pb/^{204}Pb$ and 37.018–37.241 for $^{208}Pb/^{204}Pb$.

4.4. Zircon Hf Isotopes

The zircon domains in the four samples that were dated by the U-Pb methods were also analyzed for Lu-Hf isotopes simultaneously, and the results are listed in supporting information Table S1 and Figure S2. The zircons from gabbro 09JZY14 exhibit very negative $\varepsilon_{Hf}(t)$ values of −18.4 to −21.8. The relict zircon core of Neoproterozoic U-Pb age has a negative $\varepsilon_{Hf}(t)$ value of −8.8. Eighteen analyses for gabbroic diorite 09JZY05 give variably negative $\varepsilon_{Hf}(t)$ values of −17.5 to −29.0. Gabbroic diorite 09JZY07 yields variably elevated zircon $\varepsilon_{Hf}(t)$ values of −7.7 to −20.0. For gabbroic diorite 09JZY18, twenty analyses give $\varepsilon_{Hf}(t)$ negative values of −15.4 to −23.3.

4.5. Mineral Major-Trace Elements and In-Situ Sr Isotopes

Electron microprobe data for orthopyroxene, clinopyroxene, amphibole, biotite, and plagioclase in the gabbro are presented in supporting information Tables S4 and S5. Trace elements are given in supporting information Table S6. Selected representative major and trace elements of clinopyroxene are presented in Tables 2 and 3, respectively. Representative major elements and in situ Sr isotope of plagioclase are presented in Table 4.

4.5.1. Orthopyroxene

Orthopyroxene is only present in the gabbro as big crystals without zoning. It has SiO_2 contents of 52.23–53.14 wt.% and Mg# values of 64.5–65.7 (supporting information Table S4). As shown in supporting information Figure S3a, it is enriched in LREE, with negative Eu anomalies (Eu/Eu* = 0.31–0.62). It also exhibits

Table 1. The Whole-Rock Major-Trace Element and Sr-Nd-Pb Isotope Compositions of Jiaoziyan Mafic Rocks From the Dabie Orogen

	Gabbro									Gabbroic Diorite					
Sample	09JZY10	09JZY11	09JZY12	09JZY13	09JZY14	09JZY15	09JZY16	09JZY17	09JZY19	09JZY03	09JZY04	09JZY05	09JZY07	09JZY09	09JZY18
Major Elements (wt.%)															
SiO_2	48.20	47.97	46.05	45.69	47.81	45.68	47.58	48.86	46.56	50.53	53.93	51.76	52.86	51.06	52.12
TiO_2	1.62	1.75	1.99	1.80	1.54	2.35	1.94	1.42	2.12	1.53	1.15	1.44	0.85	1.41	1.43
Al_2O_3	16.67	17.01	13.48	16.02	15.84	17.55	17.84	16.35	17.90	15.41	14.00	14.77	12.07	16.03	15.98
Fe_2O_3	10.41	10.43	13.65	12.52	10.28	11.53	10.55	9.90	10.76	8.93	8.00	9.43	5.99	8.35	9.46
MnO	0.14	0.16	0.18	0.16	0.16	0.16	0.15	0.13	0.12	0.26	0.13	0.13	0.17	0.13	0.14
MgO	4.79	5.03	6.96	5.75	6.84	4.25	3.57	5.50	3.70	5.50	5.08	5.15	6.42	3.1	4.07
CaO	8.75	7.54	8.58	10.89	7.57	7.06	7.38	9.20	7.88	7.60	6.56	6.55	8.63	5.96	8.00
Na_2O	3.76	4.01	2.66	2.80	3.64	3.65	4.31	3.67	4.21	3.35	3.41	3.47	2.66	4.22	4.07
K_2O	1.17	2.49	1.84	0.87	2.55	2.95	2.51	1.08	1.60	2.34	2.28	2.70	4.90	3.49	1.18
P_2O_5	0.99	0.91	0.77	0.35	0.74	1.20	1.15	0.86	1.15	0.67	0.51	0.64	1.15	0.67	0.92
SO_3	0.10	0.60	0.37	0.91	0.26	0.27	0.36	0.28	0.56	0.03	0.26	0.25	0.03	0.14	0.15
Total	96.6	97.9	96.5	97.8	97.2	96.7	97.3	97.3	96.6	96.1	95.3	96.3	95.7	94.6	97.5
Mg#	50.4	51.5	52.9	50.3	59.5	44.8	42.7	55.1	43.1	57.6	58.3	54.6	70.3	45.0	48.7
Trace Elements (ppm)															
Ba	1066	2001	1073	528	2483	2075	2606	949	1629	1353	1395	1437	1184	2570	1000
Rb	26.9	57.3	43.9	17.2	71.1	68.6	50.0	21.5	31.7	59.9	47.3	66.9	122	72.4	27.5
Sr	1124	1040	858	922	1179	1117	1289	1131	1284	867	718	798	669	879	1167
Ta	0.682	0.648	0.692	0.380	0.560	0.774	0.612	0.504	0.771	0.861	0.900	1.06	0.852	1.02	1.09
Nb	14.7	19.8	14.7	6.79	17.4	20.0	16.1	11.4	17.2	17.6	17.3	18.7	17.2	22.2	19.3
Hf	1.41	2.51	2.09	2.08	3.34	1.45	2.80	1.47	2.02	4.17	3.02	2.68	5.90	2.51	1.68
Zr	52.5	118	68.0	72.2	154	64.4	144	53.8	90.5	179	119	107	243	105	53.3
Y	24.9	33.5	29.1	20.0	28.4	32.4	31.9	22.4	18.9	25.7	25.4	29.4	52.9	29.0	30.2
Th	1.50	1.35	2.66	0.538	1.75	1.40	1.65	1.30	1.63	4.61	7.13	9.81	11.1	4.85	4.82
U	0.181	0.222	0.445	0.108	0.208	0.242	0.246	0.154	0.212	0.933	0.892	1.81	2.50	0.851	0.710
Cr	39.4	91.5	79.7	69.3	87.9	2.68	8.48	60.1	11.6	181	171	84.0	376	53.2	75.7
Ni	65.4	50.1	81.7	56.5	138	9.12	9.98	91.3	15.1	74.9	79.2	63.9	121	26.0	33.6
Sc	19.0	19.0	24.2	25.8	21.7	14.3	15.2	20.3	12.4	18.2	19.0	17.0	17.8	15.7	17.7
V	220	173	262	357	195	176	153	212	171	174	148	173	118	135	175
Cu	43.6	42.2	44.8	55.1	38.4	18.5	21.4	50.1	27.5	15.6	33.7	43.9	6.86	21.6	28.6
Pb	7.04	8.31	5.87	3.03	9.00	5.43	6.94	6.46	7.44	14.4	11.2	11.5	17.3	12.7	9.91
Zn	107	133	130	94.5	123	111	122	100	108	181	91.6	98.2	104	107	96.8
Li	10.9	8.64	8.02	5.29	14.8	6.80	6.31	8.14	20.1	14.5	11.3	18.9	26.8	8.81	12.7
Co	37.9	33.8	54.2	48.1	46.7	33.0	27.5	40.5	27.5	32.7	30.1	35.7	25.2	21.9	28.8
Ga	22.9	24.6	20.1	20.6	24.0	23.1	24.5	21.7	24.3	20.8	20.3	21.4	18.1	23.8	22.0
REE (ppm)															
La	60.2	84.4	48.5	20.7	75.9	64.6	75.0	51.4	71.6	56.6	68.7	70.6	88.6	70.3	77.7
Ce	116	167	101	45.2	148	134	149	101	132	112	130	138	194	137	153
Pr	13.9	20.1	12.8	6.02	17.5	16.7	18.3	12.1	15.0	13.3	14.9	15.8	24.6	16.3	17.9
Nd	54.3	78.1	52.7	26.8	68.1	66.4	73.7	47.6	57.3	52.0	56.1	59.3	104	63.0	69.9
Sm	9.33	13.0	10.3	5.87	11.4	12.2	12.7	8.37	9.04	9.42	9.13	10.5	22.7	11.2	12.3
Eu	2.67	3.47	2.69	1.97	3.01	3.76	3.76	2.42	3.02	2.67	2.41	2.62	5.29	3.02	2.96
Gd	7.56	10.3	8.75	5.38	8.99	10.4	10.3	6.82	6.96	7.66	7.27	8.50	20.2	9.01	9.56
Tb	0.990	1.37	1.18	0.747	1.19	1.40	1.33	0.918	0.844	1.02	0.975	1.13	2.54	1.18	1.24
Dy	5.07	6.88	6.01	4.01	5.90	6.77	6.42	4.60	4.07	5.37	5.00	5.86	11.6	5.96	6.30
Ho	0.848	1.15	1.00	0.714	1.00	1.13	1.12	0.788	0.662	0.885	0.858	1.01	1.72	0.988	1.07
Er	2.25	3.01	2.63	1.86	2.61	2.86	2.92	2.05	1.65	2.32	2.29	2.62	3.99	2.59	2.71
Tm	0.290	0.374	0.338	0.254	0.341	0.345	0.370	0.277	0.194	0.293	0.328	0.349	0.493	0.327	0.350
Yb	1.72	2.24	2.04	1.49	1.94	1.94	2.15	1.57	1.19	1.83	1.96	2.25	2.86	1.89	2.05
Lu	0.262	0.312	0.307	0.222	0.300	0.288	0.333	0.238	0.177	0.269	0.291	0.317	0.424	0.281	0.299
Y	24.9	33.5	29.1	20.0	28.4	32.4	31.9	22.4	18.9	25.7	25.4	29.4	52.9	29.0	30.2
$(La/Yb)_N$	25.1	27.0	17.1	10.0	28.1	23.9	25.0	23.4	43.1	22.2	25.1	22.5	22.2	26.6	27.2
Eu/Eu*	0.97	0.92	0.87	1.07	0.91	1.02	1.01	0.98	1.16	0.96	0.90	0.85	0.75	0.92	0.84
$(^{87}Sr/^{86}Sr)_i$	0.70783	0.70753	0.70715	0.7066	0.70751	0.70684	0.70779	0.70784	0.70743	0.70718	0.70774	0.70733	0.70743	0.70737	0.7076
$\varepsilon_{Nd}(t)$	−17.6	−16.2	−14.9	−10.1	−15.4	−10.9	−15.6	−17.2	−17.2	−10.2	−16.1	−13.8	−5.2		−16.2
$(^{206}Pb/^{204}Pb)_i$	16.1213	16.1712	16.2048	16.6063	16.3776	16.3001	16.197	16.1317	16.1781	16.3086	16.3455	16.4026	16.2247		16.154
$(^{207}Pb/^{204}Pb)_i$	15.2928	15.2727	15.314	15.3484	15.3544	15.3242	15.2731	15.317	15.3385	15.3302	15.5236	15.3868	15.3069		15.3083
$(^{208}Pb/^{204}Pb)_i$	37.0073	36.868	36.753	37.2324	37.21	37.1299	36.9198	37.0487	37.1547	37.1016	37.1401	37.2412	37.0231		37.0179

[a] Mg# $= 100 \times MgO/(MgO + 0.9 \times Fe_2O_3)$, $Eu^* = Eu_N/(Sm_N \times Nd_N)^{1/2}$

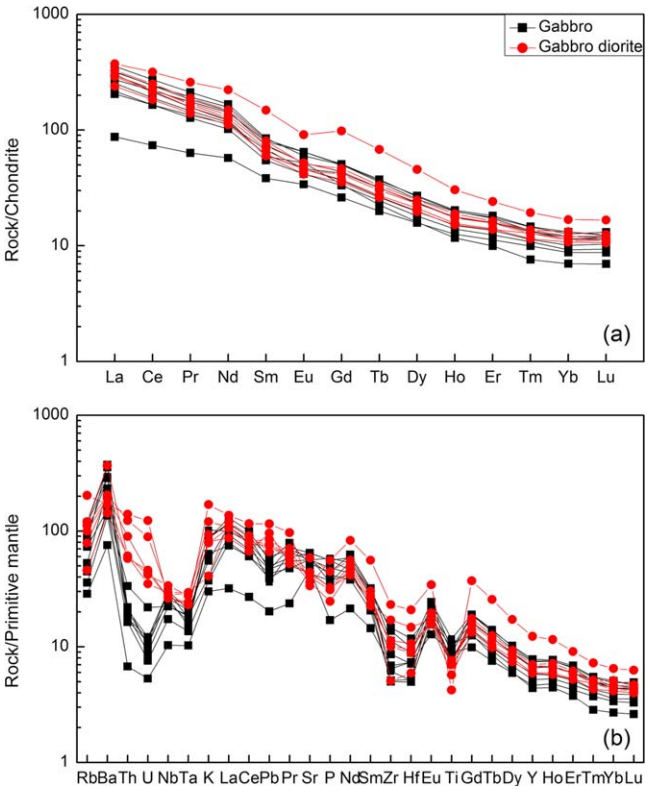

Figure 4. Diagrams of trace element compositions for the Jiaoziyan mafic rocks in the Dabie orogen. (a) Chondrite-normalized REE patterns, and (b) primitive mantle-normalized trace element spidergrams. The chondrite REE values are after *Sun and McDonough* [1989], and primitive mantle trace element values are after *McDonough and Sun* [1995].

negative Pb and Sr anomalies on the primitive mantle-normalized trace element spidergram (supporting information Figure S3b).

4.5.2. Clinopyroxene

Clinopyroxene is dominated by salite and augite, and exhibits variable major and trace compositions(supporting information Tables S4, S5 and Figure S4). Zoned and unzoned clinopyroxene megacrystals coexist in the gabbro samples. These clinopyroxene megacrystals provide detailed records of the geochemical evolution during the fractional crystallization of gabbroic magmas. Major and trace element variations across one zoned clinopyroxene megacrystal (Cpx-1 in 09JZY14), four unzoned clinopyroxene megacrystals (Cpx-2 in 09JZY11 and 09JZY14) that were replaced/unreplaced by amphibole at the rim, and several clinopyroxene grains in matrix are described below.

Cpx-1 is a relatively euhedral megacrystal in gabbro 09JZY14. From core to rim of profile A-B (Figures 2b and 5), Mg# values decrease from 78.4–80.4 in Cpx-1 core, 77.4–78.9 in Cpx-1 mantle, to 74.9–76.9 in Cpx-1 rim. SiO_2 contents decrease from 51.50–52.78 wt.% in Cpx-1 core and 50.61–51.66 wt.% in Cpx-1 mantle, and then increase to 51.72–52.85 wt.% in Cpx-1 rim. In contrast, Al_2O_3, TiO_2, Cr and Ni contents increase from 1.66–2.12 wt.%, 0.32–0.39 wt.%, 63–847 ppm, and 82–163 ppm in Cpx-1 core, to 2.36–3.72 wt.%, 0.52–0.87 wt.%, 1198–3521 ppm and 147–175 ppm in Cpx-1 mantle, and then decrease rapidly to 1.40–1.83 wt.%, 0.20– 0.31 wt.%, 14.2–643 ppm, and 65.4–105 ppm in Cpx-1 rim, respectively (supporting information Figures S5a, S5b, and S6). Compared to Cpx-1 rim and Cpx-1 mantle, Cpx-1 core has significantly high contents of Rb (0.12–0.94 ppm) and Ba (2.97–176 ppm). As shown in supporting information Figure S3a, they exhibit similar REE patterns with LREE enrichment. While Cpx-1 rim has significantly negative Eu anomalies (Eu/Eu* = 0.31–0.62), Cpx-1 core (Eu/Eu* = 0.76–1.05) and Cpx-1 mantle (Eu/Eu* = 0.82–1.16) are not obvious in Eu anomalies. On the primitive mantle-normalized trace element spidergram (supporting information Figure S3b), they exhibit similar features with depletion of Pb, P and HFSE (Nb, Ta, Zr, Hf and Ti). Cpx-1 core is significantly enriched in Rb, Ba and K relative to Cpx-1 mantle and Cpx-1 rim (Figures 5f–5h).

Four Cpx-2 megacrystals without clear zoning from gabbros 09JZY11 and 09JZY14 were also investigated. There are often replacements by amphibole at the rim in gabbro 09JZY14 (Figures 2c and 2d). These Cpx-2 megacrystals exhibit variable Mg# values (71.3–77.3), Al_2O_3 (1.24–4.05 wt.%) and TiO_2 (0.19–0.85 wt.%). On the chondrite-normalized REE diagram (supporting information Figure S3a), they exhibit LREE enrichment with $(La/Yb)_N$ = 3.6–6.7 and negative to no Eu anomalies (Eu/Eu* = 0.61–1.01). Similar to Cpx-1 mantle, Cpx-2 crystals also have high contents of Cr (709–2947 ppm) and Ni (71–172 ppm) (supporting information Figure S6 and Table S6) but low contents of Rb and Ba.

Clinopyroxene grains in matrix have Mg# values of 73.1–77.1 and low contents of Al_2O_3 (1.03–1.71 wt.%), TiO_2 (0.13–0.29 wt.%), Cr (6.7–55.2 ppm) and Ni (55.3–75.6 ppm) (supporting information Figures S5a, S5b, and S6). They are also characterized by LREE enrichment with negative Eu anomalies (Eu/Eu* = 0.63–0.83), but relative depletion of Rb, Ba, Pb, P, Zr, Hf and Ti (supporting information Figures S3a and S3b).

Table 2. Representative Major Elements of Clinopyroxene From the Jiaoziyan Mafic Rocks in the Dabie Orogen

Grain	Cpx-1									Cpx-2						Cpx in Matrix				
Position	Cpx-1 Rim			Cpx-1 Mantle			Cpx-1 Core													
Spot	1	2	3	8	9	10	19	20	21	15	16	9	10	3	4	1	2	3	4	5
SiO_2	51.72	52.18	52.85	50.96	50.61	51.37	52.26	52.11	52.10	51.19	51.13	51.41	50.35	50.81	50.81	53.11	53.70	53.18	51.73	52.53
TiO_2	0.31	0.27	0.20	0.66	0.73	0.64	0.36	0.36	0.39	0.36	0.50	0.38	0.79	0.82	0.74	0.16	0.13	0.23	0.18	0.17
Al_2O_3	1.83	1.83	1.40	3.08	3.22	2.74	2.12	2.11	1.98	2.22	2.70	2.25	3.61	3.44	3.07	1.14	1.03	1.47	1.12	1.00
Cr_2O_3				0.24	0.36	0.23	0.05		0.05	0.30	0.30	0.24	0.28	0.40	0.30	0.04	0.01	0.01		
FeO	8.01	8.40	7.85	7.62	7.61	7.38	7.24	7.21	7.34	8.92	8.89	8.39	9.46	8.34	8.42	8.29	8.27	8.33	9.08	9.45
MnO	0.34	0.32	0.41	0.25	0.26	0.28	0.20	0.26	0.22	0.40	0.42	0.37	0.31	0.39	0.41	0.48	0.52	0.41	0.52	0.52
MgO	13.37	13.89	14.13	14.76	14.67	14.78	15.33	15.17	15.31	14.26	14.37	14.72	14.59	13.59	13.71	14.57	14.08	14.27	13.82	14.04
CaO	22.10	21.83	21.97	21.27	21.16	21.28	21.30	21.45	21.34	20.86	20.13	21.02	18.79	21.74	21.53	21.80	22.01	22.16	21.81	21.61
Na_2O	0.61	0.53	0.52	0.68	0.66	0.60	0.60	0.66	0.63	0.71	0.88	0.69	0.98	0.58	0.58	0.46	0.49	0.46	0.40	0.42
K_2O	0.01	0.01	0.01		0.01	0.01			0.01		0.11	0.03	0.21	0.07	0.07	0.00	0.00	0.02	0.00	0.00
Total	98.30	99.25	99.34	99.52	99.29	99.31	99.47	99.32	99.37	99.22	99.42	99.50	99.37	100.17	99.65	100.04	100.26	100.54	98.64	99.73
Mg#	75.0	74.9	76.4	77.7	77.6	78.3	79.2	79.1	79.0	74.2	74.4	76.0	73.5	74.6	74.6	76.0	75.4	75.5	73.3	72.8
Fs	47.0	45.7	45.9	12.38	12.44	12.04	11.63	11.61	11.78	14.52	14.66	13.55	15.79	13.7	13.9	13.25	13.36	13.33	14.6	15.1
Wo	39.8	40.7	41.3	44.44	44.43	44.61	44.02	44.40	44.00	43.67	42.69	43.64	40.35	46.0	45.5	44.82	45.70	45.57	45.2	44.5
En	13.2	13.7	12.7	43.18	43.14	43.36	44.35	43.98	44.22	41.81	42.65	42.80	43.86	40.3	40.6	41.93	40.94	41.10	40.1	40.4

Table 3. Representative Trace Elements of Clinopyroxene From the Jiaoziyan Mafic Rocks in the Dabie Orogen

Grain	Cpx-1									Cpx-2						Cpx in Matrix				
Position	Cpx-1 Rim			Cpx-1 Mantle			Cpx-1 Core													
Spot	1	2	3	8	9	10	19	20	21	6	7	3	4	1	2	1	2	3	4	5
Cr	14.2	15.7	19.9	2262	2378	1854	377	426	193	2277	2552	1778	1936	2947	2384	11.5	15.4	10.5	8.21	8.66
Co	30.6	32.5	31.8	30.8	32.6	33.4	32.6	33.9	39.5	34.7	32.4	34.1	32.3	29.2	29.2	30.9	31.6	34.6	36.2	33.0
Ni	65.4	71.5	69.0	155	150	157	81.6	82.3	110	80.4	85.1	171	172	98.3	106	37.4	33.1	70.5	75.6	72.5
Zn	91.3	97.5	93.6	83.6	77.9	73.1	68.0	62.1	75.7	123	136	113	106	110	116	114	130	117	110	117
Ga	6.33	7.28	6.81	8.93	8.89	8.50	7.03	6.85	8.88	8.96	8.85	7.89	8.10	11.9	10.9	6.91	6.97	5.89	6.12	9.00
Rb	0.31	0.15		0.11	0.12	0.044	4.63	9.41	2.15	0.35	0.18	0.43	0.79	0.0025	0.72	0.088	0.15		0.077	0.031
Ba	4.27	2.05	0.25	5.99	5.12	6.03	75.3	176	96.3	16.3	4.83	6.61	13.6	18.5	23.7	0.48		0.15	0.54	0.49
Th	0.16	0.22	0.15	0.30	0.22	0.26	0.24	0.24	0.67	0.32	0.29	0.40	0.32	0.39	0.14	0.14	0.032	0.054	0.093	0.12
U	0.023		0.005	0.027	0.024	0.025	0.021	0.42	0.009	0.0002	0.034	0.018	0.020	0.040	0.082			0.017		0.014
Nb	0.25	0.13	0.16	0.50	0.32	0.41	0.048	0.021	0.95	1.85	0.91	0.57	1.00	2.18	2.68	0.10	0.079	0.055	0.090	0.11
Ta	0.037	0.014	0.021	0.009	0.013	0.035	0.007		0.049	0.045	0.033	0.022	0.025	0.073	0.071		0.026			0.013
K	64	61	1.7	257	180	118	2141	1357	4204	586	252	269	550	563	755		11.2	3	6	3
La	20.9	23.1	22.6	18.6	17.1	17.1	8.10	8.88	13.7	21.8	19.8	21.7	22.8	32.2	28.3	22.1	23.5	17.2	17.2	22.9
Ce	78.2	86.2	83.9	54.2	48.4	49.4	23.2	24.0	33.7	72.6	68.9	72.1	74.7	124	105	89.1	95.5	66.3	66.1	89.9
Pb	1.16	1.80	1.05	0.93	0.84	0.91	1.16	1.00	1.57	0.7501	0.9067	0.768	0.8333	0.89	1.10	1.15	0.56	0.75	0.90	0.89
Pr	13.2	14.5	14.2	7.33	6.76	6.27	3.76	3.70	5.21	11.3	10.9	10.3	10.3	18.5	15.4	15.6	16.8	10.3	10.7	14.3
Sr	57.0	57.7	55.9	78.1	80.0	83.7	95.8	86.8	119	61.4	59.2	60.2	64.6	57.0	61.3	38.0	40.3	48.1	47.4	52.1
P	27.3	34.0	25.5	69.6	67.9	39.9	47.0	41.3	71.3	29.4	22.4	40.9	47.4	57.3	28.8	15.1	19.1	26.3	83.1	42.3
Nd	64.2	70.3	66.2	36.6	32.4	34.2	20.0	20.1	27.9	55.1	51.9	41.5	45.5	65.3	61.1	82.5	80.8	52.6	52.6	67.0
Sm	16.8	16.0	17.8	9.14	7.64	7.47	5.95	4.60	7.56	12.7	11.9	8.86	9.52	14.5	16.1	23.2	25.0	12.2	12.2	16.4
Zr	79.1	63.7	65.2	68.8	66.4	62.1	75.6	74.7	94.4	56.9	60.5	50.5	50.9	66.4	70.8	31.8	33.2	27.1	23.3	116
Hf	3.93	3.34	3.35	2.32	2.28	2.18	2.48	2.50	4.26	2.52	2.69	1.57	1.57	2.68	2.74	2.15	1.89	1.25	1.19	7.30
Eu	3.39	3.57	3.79	2.60	2.30	2.10	1.56	1.21	1.81	2.70	2.70	2.52	2.59	4.19	2.99	2.71	3.09	2.66	2.59	3.53
Ti	1075	1136	1147	4740	4558	4578	1703	1727	4223	2760	2454	2721	2716	4870	4445	918	909	794	796	1800
Gd	14.1	16.1	16.5	8.21	6.92	7.10	5.22	4.83	6.58	9.64	10.7	6.55	7.40	11.4	13.8	21.3	19.7	9.67	10.5	13.1
Tb	2.30	2.35	2.54	0.96	1.03	0.88	0.73	0.70	0.98	1.49	1.32	0.92	1.10	1.49	1.63	3.64	3.41	1.29	1.47	1.92
Dy	13.0	12.7	13.1	5.83	5.43	5.31	4.12	4.17	5.37	7.81	7.73	5.27	5.42	10.6	13.4	24.9	19.3	7.87	7.89	11.3
Y	56.1	58.8	57.6	26.2	24.0	24.9	17.5	17.4	22.0	37.6	36.9	25.9	27.0	52.6	51.2	80.5	86.8	33.9	36.1	47.0
Ho	2.01	2.20	2.21	1.09	0.92	0.91	0.67	0.76	0.93	1.43	1.49	1.20	1.17	1.81	2.04	3.03	3.32	1.38	1.48	2.11
Er	5.71	6.09	5.80	2.48	2.44	2.10	1.55	1.50	2.30	3.46	4.02	2.55	2.55	4.53	6.22	9.08	9.74	3.36	3.65	4.80
Tm	0.62	0.76	0.92	0.34	0.31	0.33	0.24	0.23	0.29	0.50	0.47	0.41	0.39	0.59	0.66	1.24	1.12	0.37	0.46	0.63
Yb	4.58	4.85	5.01	2.13	1.97	1.58	1.34	1.13	1.83	3.09	3.42	2.33	2.71	4.61	4.36	8.82	7.96	3.24	2.36	4.01
Lu	0.71	0.76	0.79	0.25	0.25	0.29	0.22	0.20	0.26	0.51	0.52	0.34	0.34	0.85	0.73	1.11	1.10	0.39	0.43	0.57
$(La/Yb)_N$	3.28	3.42	3.23	6.27	6.23	7.78	4.32	5.62	5.36	5.06	4.16	6.68	6.04	5.01	4.66	1.79	2.12	3.81	5.24	4.10
Eu/Eu*	0.67	0.68	0.68	0.92	0.97	0.88	0.86	0.79	0.78	0.75	0.73	1.01	0.94	1.00	0.61	0.37	0.42	0.75	0.70	0.74

Table 4. Representative Major Elements and Rb-Sr Isotopes of Plagioclase From the Jiaoziyan Mafic Rocks (09JZY11) in the Dabie Orogen[a]

	Pl-1 From 09JZY11											
Position	Pl-1 Core				Pl-1 Mantle				Pl-1 Rim			
Spot	1	2	3	4	5	6	7	8	9	10	11	12
SiO_2	58.24	57.82	58.06	58.61	55.21	56.14	54.11	54.7	61.24	61.22	61.46	60.32
Al_2O_3	25.8	27.51	25.35	25.93	28.25	28.57	28.05	28.7	24.55	24.05	24.63	24.94
MgO	0.02			0.01			0.01	0.01				
CaO	8.39	8.82	8.67	7.82	10.83	11.39	11.35	11.39	6.81	6.34	6.29	6.29
Na_2O	6.13	6.32	7.18	6.97	4.85	4.39	4.913	5.03	7.45	7.63	7.62	7.89
K_2O	0.42	0.39	0.4	0.42	0.27	0.23	0.23	0.2	0.51	0.57	0.5	0.56
Total	99	100.86	99.66	99.76	99.42	100.71	98.66	100.02	100.55	99.81	100.5	100
An	42	42.6	39.2	37.4	54.4	58.1	55.4	55	32.6	30.5	30.5	29.7
Ab	55.5	55.1	58.6	60.2	44	40.5	43.3	43.9	64.5	66.2	66.6	67.2
Or	2.5	2.3	2.2	2.4	1.6	1.4	1.3	1.1	2.9	3.2	2.9	3.1
$^{87}Rb/^{86}Sr$	0.0018	0.0024	0.0264	0.0164	0.0018	0.0016	0.0013		0.0123		0.0075	
2σ	0.0001	0.0002	0.001	0.0007	0.0001	0.0001	0.0001		0.0005		0.0007	
$^{87}Sr/^{86}Sr$	0.7075	0.70769	0.70768	0.70778	0.70739	0.70758	0.70756		0.70772		0.70789	
2σ	0.00019	0.00017	0.00017	0.00018	0.00018	0.00017	0.00018		0.00021		0.00018	
$(^{87}Sr/^{86}Sr)_i$	0.70749	0.70769	0.70763	0.70775	0.70739	0.70757	0.70755		0.70769		0.70788	

	Pl-2 from 09JZY11						Pl in Matrix from 09JZY11			
Position	Pl-2 core			Pl-2 rim						
Spot	1	2	3	4	5	6	1	1	1	1
SiO_2	53.56	53.34	52.71	61.99	60.45	62.17	61.85	60.02	61.3	61.85
Al_2O_3	29.26	29.72	29.08	24.44	23.96	23.51	23.42	24.87	24.57	23.43
MgO	0.02	0.11	0.36		0.01	0.01		0.01	0.02	0.01
CaO	12.1	11.61	12.21	6.34	6.31	6.51	6.31	6.96	6.98	6.55
Na_2O	4.27	4.81	3.97	7.57	7.71	7.52	7.55	7.55	6.58	7.68
K_2O	0.23	0.31	0.49	0.55	0.51	0.47	0.58	0.4	0.51	0.5
Total	99.43	99.9	98.82	100.9	98.94	100.2	99.71	99.8	99.96	100
An	60.3	56.2	61.2	30.7	30.3	31.5	30.6	33	35.8	31.2
Ab	38.4	42.1	35.9	66.2	66.8	65.8	66.1	64.7	61.1	66
Or	1.4	1.8	2.9	3.2	2.9	2.7	3.4	2.2	3.1	2.8
$^{87}Rb/^{86}Sr$	0.0028	0.0025	0.0023	0.0089	0.0514	0.0055	0.0172	0.0476	0.0158	0.1813
2σ	0.0001	0.0001	0.0001	0.0005	0.0006	0.0004	0.0004	0.0014	0.0006	0.0041
$^{87}Sr/^{86}Sr$	0.70728	0.70728	0.70755	0.70762	0.70777	0.70779	0.70785	0.7079	0.70764	0.70817
2σ	0.00021	0.0002	0.00018	0.00021	0.00018	0.00018	0.00016	0.00018	0.00018	0.00022
$(^{87}Sr/^{86}Sr)_i$	0.70727	0.70727	0.70755	0.7076	0.70768	0.70778	0.70782	0.70781	0.70761	0.70784

[a]The initial Sr isotopic ratios are calculated at t = 128 Ma.

4.5.3. Amphibole

The investigated amphiboles are mainly magnesiohastingsite and edenite in the calcic amphibole group of *Leake et al*. [1997], with subordinately tschermakite. Amphiboles in Cpx-1 core (hereafter Amp-1) have high Mg# values of 66.4–67.3 (supporting information Table S4; Figures S5c and S5d), with high contents of Al_2O_3 (10.47–10.80 wt. %) and TiO_2 (2.49–2.87 wt. %). They have Cr and Ni contents of 566–609 ppm and 213–218 ppm (supporting information Figure S6), respectively. As shown in supporting information Figure S3c, they are characterized by LREE enrichment with negative Eu anomalies (Eu/Eu* = 0.71–0.74, supporting information Table S6). On the primitive mantle-normalized trace element spidergram (supporting information Figure S3d), they show depletion of U, Pb, P, Zr, Hf and Ti.

Amp-2 (amphibole growing around Cpx-2) and amphibole in matrix have similar element features (supporting information Figures S5c, S5d and Table S4). They have relatively low contents of Mg# (61.5–65.9), Al_2O_3 (8.66–9.94 wt.%) and TiO_2 (1.71–2.38 wt.%). Compared to Amp-1, they have significantly low contents of Cr (22.4–263 ppm) and Ni (111–141 ppm). They are also characterized by LREE enrichment and negative Eu anomalies, but with significantly high REE contents (supporting information Figure S3c).

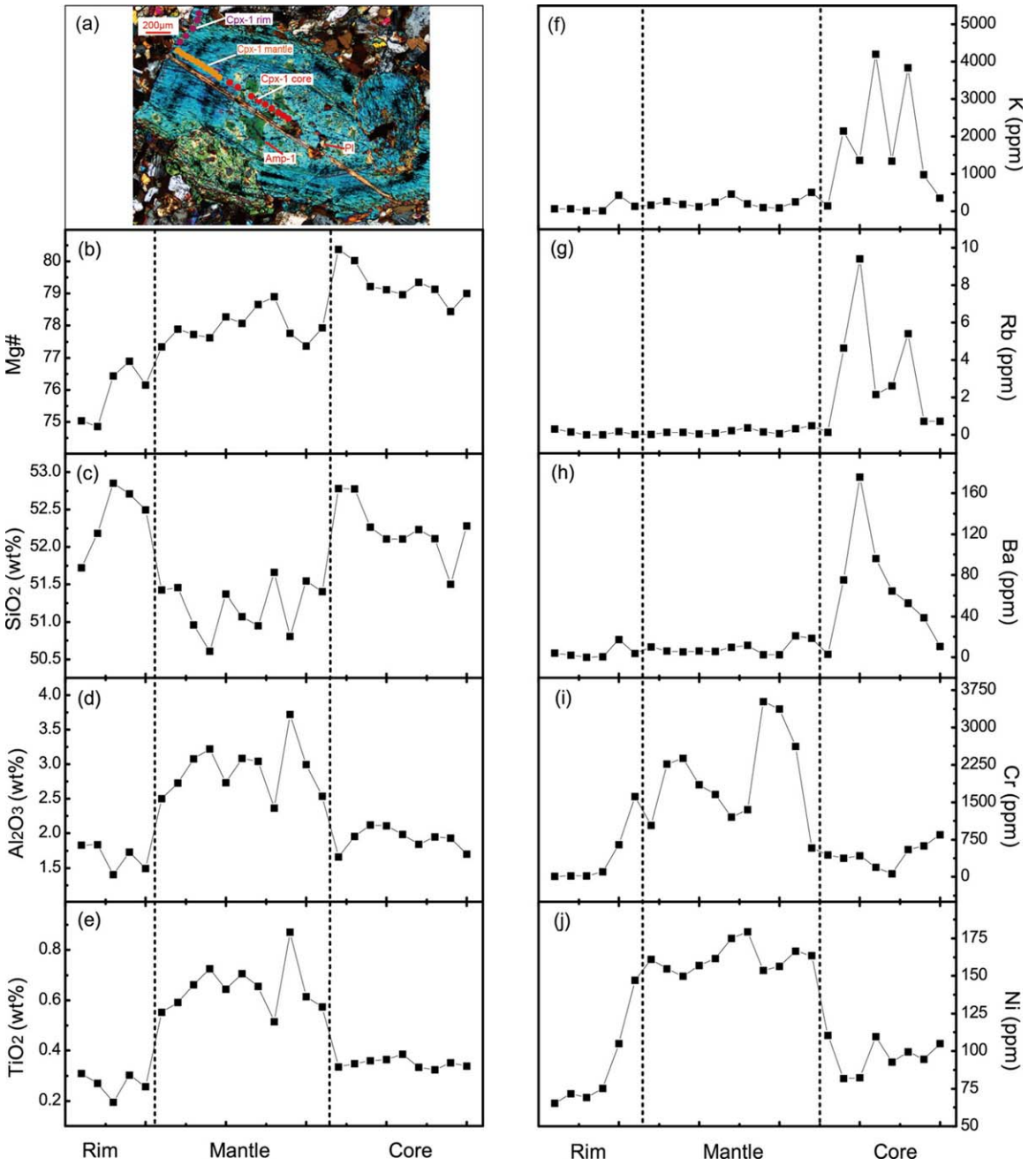

Figure 5. Compositional profile across a large clinopyroxene megacrystal (Cpx-1) with clear zoning from core to rim in gabbro 09JZY14.

4.5.4. Plagioclase and Mineral Inclusions

Plagioclase in the gabbro exhibits variable element and isotope compositions (Table 4). Also analyzed were major elements and Sr isotopes across Pl-1 and Pl-2 megacrystals in sample 09JZY11, and several plagioclase grains in matrix.

Pl-1 exhibits clear zoning with core-mantle-rim structures (Figure 2g). From core to rim, An values increase rapidly from 37.4–42.6 in Pl-1 core to 54.4–58.1 in Pl-1 mantle, then decrease to 29.7–32.6 in Pl-1 rim (Table 4, Figures 6b and 7). Meanwhile, initial $^{87}Sr/^{86}Sr$ ratios decrease from 0.70749–0.70775 in Pl-1 core to 0.70739–0.70755 in Pl-1 mantle, and then increase to 0.70769–0.70788 in Pl-1 rim (Figures 6c and 7). Pl-2 displays clearly core-rim structures. An values decrease from 56.2–61.2 in Pl-2 core to 30.3–31.5 in Pl-2 mantle (Figure 7). Initial $^{87}Sr/^{86}Sr$ ratios of Pl-2 increase from 0.70727–0.70755 in Pl-2 core to 0.70760–0.70778 in

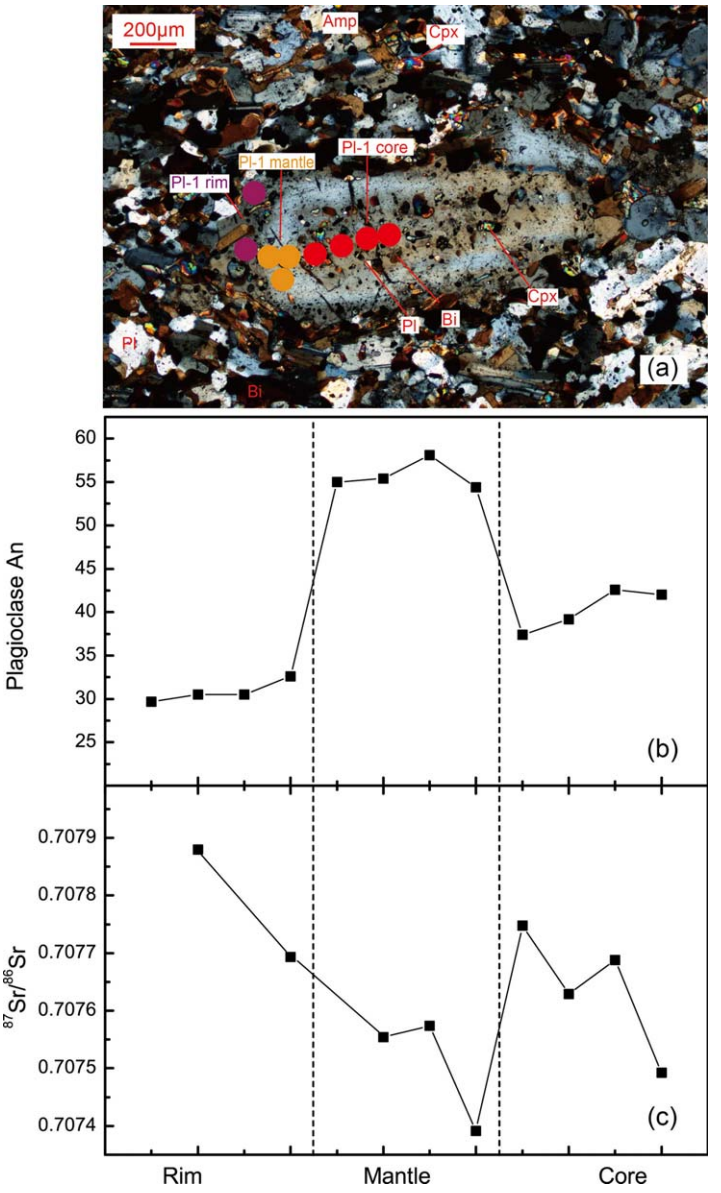

Figure 6. Compositional profile across a large plagioclase megacrystal (Pl-1) with clear zoning from core to rim in Jiaoziyan gabbro 09JZY11.

Pl-2 rim. Plagioclase grains in the matrix generally have An values of 30.6–35.8 and initial $^{87}Sr/^{86}Sr$ ratios of 0.70761–0.70784, similar to those of Pl-1 rim and Pl-2 rim. Generally, plagioclase in gabbro exhibits significantly compositional variations according to plot of plagioclase An values versus initial Sr isotope ratios (Figure 7), although plagioclase in situ Sr isotopes display limited range.

Plagioclase inclusions in Pl-1 core were also analyzed for major elements, yielding An = 31.5, similar to that of plagioclase inclusion (An = 35.2) in Cpx-1 core (supporting information Table S5). Clinopyroxene inclusions in Pl-1 core also have similar Mg#, Al_2O_3 and TiO_2 to those of Cpx-1 core (supporting information Table S4). Plagioclase inclusions in Amp-2 have low An values of 27.9–31.8, similar to those of plagioclase grains in the matrix (supporting information Table S5). Biotite inclusions in Pl-1 core have MgO and FeO contents of 13.5 wt.% and 15.8 wt.% (supporting information Table S4). Biotite grains in the matrix have MgO and FeO contents of 13.5–15.2 wt. % and 14.8–16.2 wt. %, respectively.

5. Discussion

The present zircon U-Pb dating yields relatively consistent ages of 126 ± 1 to 130 ± 1 Ma for the Jiaoziyan mafic rocks (Figure 3). These U-Pb ages are in agreement with known ages for postcollisional magmatism in the Dabie-Sulu orogenic belt [*Zhao and Zheng*, 2009]. Furthermore, gabbro 09JZY14 contains a relict zircon core with an U-Pb age of 765 ± 8 Ma, which is also consistent with Neoproterozoic protolith U-Pb ages for UHP metaigneous rocks in the Dabie-Sulu orogenic belt [*Zheng et al*., 2004; *Tang et al*., 2008a, 2008b; *Zhao et al*., 2008]. Relict zircon cores of the mid-Neoproterozoic U-Pb ages also have been identified in postcollisional mafic-ultramafic rocks at Daoshichong and Zhujiapu in the Dabie orogen [*Dai et al*., 2011, 2012]. Therefore, both the postcollisional igneous rocks and the UHP metaigneous rocks share the same parental rocks of Neoproterozoic age, which have a tectonic affinity to the subducted South China Block [*Zhao and Zheng*, 2009; *Zheng et al*., 2009]. These mafic rocks exhibit initial $^{206}Pb/^{204}Pb$ ratios of 16.121–16.606 (Table 1), similar to those of UHP metaigneous rocks in the Dabie orogen [*Zhang et al*. 2002; *Huang et al*. 2007; *Zhao and Zheng*. 2009]. This also lends support to involvement of the subducted continental crust of the South China Block in the mantle source of postcollisional mafic igneous rocks.

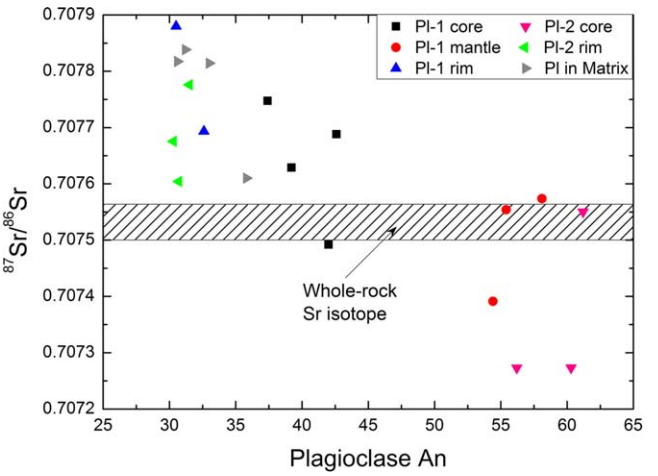

Figure 7. Plot of plagioclase An values versus initial Sr isotope ratios in Jiaoziyan gabbro 09JZY11.

Source heterogeneity and magma mixing are two important variables to dictate the composition of igneous rocks in continental collisional orogens. They have been widely recognized by field observations, whole-rock and mineral geochemical studies of both plutonic and volcanic rocks [e.g., *Keay et al*., 1997; *Maclennan et al*., 2003; *Bonin*, 2004; *Yang et al*., 2007; *Winpenny and Maclennan*, 2011]. While the source heterogeneity is realized by the source mixing of different components in the source, the magma mixing is the mixing between two or more melt batches to form a hybrid magma during melt transport and emplacement. Both the source and magma mixing processes can result in heterogeneous compositions of whole-rock and mineral elements and isotopes [e.g., *Carr et al*., 1990; *Barbarin*, 2005; *Sun et al*., 2010; *Neave et al*., 2013]. Thus, it is crucial to identify the nature of source and magma mixing processes when deciphering the petrogenesis of igneous rocks. However, traditional studies of powdered whole-rock geochemistry cannot provide diagnostic information on the distinction between the two processes.

Microbeam in situ analysis on different domains of individual minerals has the advantage over the whole-rock analyses to trace the magma mixing in addition to the source mixing [*Davidson et al*., 2007; *Tiepolo and Tribuzio*, 2008; *Sun et al*., 2010]. Pyroxene and amphibole, which are common in mafic igneous rocks and relatively rich in many trace elements, often play an important role in doing so. Several recent studies have indicated the applicability of clinopyroxene and amphibole in situ analyses to identification of magmatic processes [e.g., *Guo et al*., 2007; *Tiepolo and Tribuzio*, 2008; *Winpenny and Maclennan*, 2011; *Chen et al*., 2013a]. These mafic minerals of large grains can preserve magmatic mineral inclusions, relict mineral phases and complex zoning of major and trace elements, recording the magmatic processes such as fractional crystallization and magma mixing. Thus, the in situ geochemical analyses of minerals, in coupling with whole-rock analyses, are capable of providing robust constraints on the distinction between source mixing and magma mixing during mafic magmatism. Below we examine the two processes of source mixing and magma mixing by an integrated interpretation of major and trace element data as well as stable and radiogenic isotope data.

5.1. Source Mixing for Heterogeneously Enriched Mantle Domains

The Jiaoziyan mafic rocks exhibit low SiO_2 contents of 45.7–53.9 wt.%, high MgO contents with high Mg# values (up to 70). These compositional features are significantly different from those of felsic melts produced by partial melting of crustal rocks [e.g., *Patiño Douce and Beard* 1995; *Rapp and Watson* 1995], indicating their origination from ultramafic lithology such as peridotite, pyroxenite and hornblendite. On the other hand, they exhibit arc-like trace element distribution patterns such as enrichment in LILE and LREE but depletion of HFSE (Figure 4), indicating the presence of crustal components in them. Furthermore, they display high initial $^{87}Sr/^{86}Sr$ ratios of 0.7066–0.7078 (Table 1), negative whole-rock $\varepsilon_{Nd}(t)$ values of −17.6 to −5.2 and zircon $\varepsilon_{Hf}(t)$ values of −29.0 to −7.7, also indicating the presence of crustal components in them. All these geochemical features clearly indicate involvement of the continental crust in their petrogenesis.

Generally, there are two mechanisms to incorporate crustal components into mafic melts: (1) crustal contamination of mantle-derived mafic melts during their ascent en route the continental crust (e.g., AFC process); (2) partial melting of the fertile and enriched mantle source that was previously metasomatized by crust-derived components [*Zhao et al*., 2013]. Although the Jiaoziyan mafic rocks exhibit relatively variable whole-rock $\varepsilon_{Nd}(t)$ values of −17.6 to −5.2 and zircon $\varepsilon_{Hf}(t)$ values of −29.0 to −7.7, they have similar whole-rock initial $^{87}Sr/^{86}Sr$ ratios of 0.7066 to 0.7078. Furthermore, there are no significant correlations on the diagrams of whole-rock SiO_2 contents versus $\varepsilon_{Nd}(t)$ values and $(^{87}Sr/^{86}Sr)_i$ ratios (Figures 8a and 8b). Because SiO_2 is the most mobile component in crustal rocks, SiO_2-rich melts are always produced by the first batch

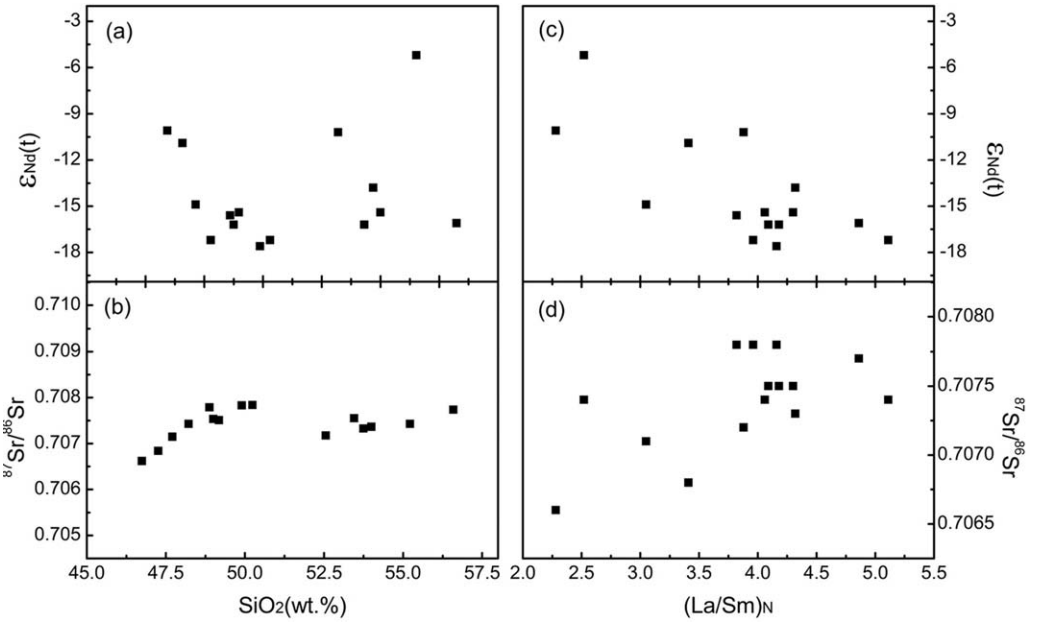

Figure 8. Plots of whole-rock geochemical variables for the Jiaoziyan mafic rocks in the Dabie orogen. (a and b) Whole-rock SiO_2 contents versus $\varepsilon_{Nd}(t)$ values and initial Sr isotope ratios, and (c and d) whole-rock $(La/Sm)_N$ ratios versus initial Nd and Sr isotope ratios.

of partial melting [*Zheng and Hermann*, 2014]. As a consequence, more SiO_2 would be incorporated into the assimilated melt in coupling with crustal Sr-Nd isotope signature if the crustal contamination did take place. However, this is not the case from our data, demonstrating that the crustal contamination did not play a significant role during the melt ascent [*Zhao et al*., 2005; *Dai et al*., 2012]. Therefore, the arc-like trace element and enriched radiogenic isotope features for the mafic rocks were inherited from their mantle source, which may be the result of source mixing between mantle and crustal components.

The Jiaoziyan mafic rocks exhibit variable whole-rock $\varepsilon_{Nd}(t)$ values of −17.6 to −5.2, precluding a simple, common evolution by the closed-system process of crystal fractionation. Instead, it suggests the source heterogeneity. A two-component mixing trend is well defined on the diagrams of whole-rock $(La/Sm)_N$ ratios versus $\varepsilon_{Nd}(t)$ values and $(^{87}Sr/^{86}Sr)_i$ ratios (Figures 8c and 8d). One endmember is characterized by high $(La/Sm)_N$ ratios with low $\varepsilon_{Nd}(t)$ values but high $(^{87}Sr/^{86}Sr)_i$ ratios, whereas the other is characterized by relatively low $(La/Sm)_N$ ratios with high $\varepsilon_{Nd}(t)$ values but low $(^{87}Sr/^{86}Sr)_i$ ratios. Such a feature suggests that the Jiaoziyan mafic rocks would be originated from a heterogeneous mantle source, which is consistent with the wide range of zircon $\varepsilon_{Hf}(t)$ values from −29.0 to −7.7. The post-collisional mafic igneous rocks in the Dabie orogen also exhibit variable zircon Hf-O isotope compositions that match a three-layer Hf-O isotope structure for the subducted continental crust of the South China Block [*Dai et al*., 2011]. Therefore, we conclude that the source mixing of the mantle peridotite with different components of the subducted continental crust is responsible for the geochemical heterogeneity in the mantle source of mafic igneous rocks.

The source mixing between the mantle peridotite and crust-derived components is common at deep oceanic subduction zones [e.g., *Ringwood*, 1990; *Zheng*, 2012; *Spandler and Pirard*, 2013]. This is generally realized by reaction of the mantle wedge peridotite with fluids/melts derived from subducting oceanic crust, yielding relatively enriched mantle domains for basaltic magmatism. *Willbold and Stracke* [2010] also proposed that source mixing of the mantle peridotite with materials derived from the continental crust and oceanic lithosphere can serve as the enriched mantle sources for ocean island basalts (OIB). This kind of metasomatic mantle sources is generally fertile in lithochemistry and enriched in melt-mobile incompatible trace elements and their radiogenic isotopes. Thus it is susceptible to partial melting relative to the refractory SCLM. The Jiaoziyan mafic rocks in the Dabie orogen exhibit arc-like trace element distribution patterns and relatively enriched radiogenic Sr-Nd-Hf isotope compositions. Such features can be attributed to geochemical inheritance from their mantle source due to the source mixing between the subducted South China Block and the overlying SCLM wedge peridotite [*Zhao et al*., 2013]. The variable whole-rock $\varepsilon_{Nd}(t)$ and

zircon $\varepsilon_{Hf}(t)$ values suggest that the mantle source is heterogeneous, which would be generated by reaction of the SCLM peridotite with felsic melts derived from partial melting of the different parts of subducted continental crust *[Dai et al*., 2011]. Therefore, the source heterogeneity is produced by the melt-peridotite reaction at the slab-mantle interface in the continental subduction channel [*Zheng et al*., 2013b].

5.2. Magma Mixing for Mineral Compositional Zoning

Besides the whole-rock geochemistry, the texture and mineral chemistry of the Jiaoziyan mafic igneous rocks also suggest their origination from a heterogeneous mantle source with significant magma mixing prior to the final emplacement. In the following discussion, we mainly focus on mineral textures and compositions that provide insights into possible magmatic components, magma mixing and evolution processes that were involved in petrogenesis of the Jiaoziyan mafic rocks.

The complex compositional variations of clinopyroxene and plagioclase megacrystals are evident in the Jiaoziyan mafic rocks (Figures 2, 5, 6, and 7), suggesting that these megacrystals experienced a complex growth history. The highly compatible elements Cr and Ni in Cpx-1 increase from core to mantle, then decrease rapidly in rim. In addition, Cpx-1 core has significantly higher Rb and Ba than those of Cpx-1 mantle and rim. The plagioclase An values of Pl-1 increase rapidly from core to mantle, then decrease in rim. On the other hand, the initial $^{87}Sr/^{86}Sr$ ratios decrease from core to rim, then increase in rim. All these features argue against their origin from the crustal contamination in open systems or the fractional crystallization in a closed system during their growth from core to mantle. This is because these processes should result in normal zonation in clinopyroxene and plagioclase rather than the reversed zonation. These features also argue against their crystallization from different batchs of magmas that were derived from the same source. Magmas of the same source should have homogeneous isotope compositions, but would not result in the variable Sr isotope ratios in plagioclase. More primitive magmas recharge to magma chamber could explain the high Ni and Cr in Cpx-1 mantle, but this process cannot explain the relatively low Mg# and high Al_2O_3 in Cpx-1 mantle. In addition, there is a wide range of zircon $\varepsilon_{Hf}(t)$ values from -29.0 to -7.7 for the Jiaoziyan mafic rocks (supporting information Table S1), also arguing for the source heterogeneity. All these arguments presented above suggest that either fractional crystallization or crustal contamination, or a combination of both in the continental crust, is unlikely to be the primary cause for the complex compositional variation in the Cpx and Pl megacrystals. They argue for the contribution of source heterogeneity to the generation of the Jiaoziyan mafic rocks.

According to the element and isotope compositions of minerals (especially Cpx, Pl and Amp) from the Jiaoziyan mafic rocks, three principal stages of mineral crystallization can be deduced during mafic magmatism. The first stage is documented in the Cpx-1 core and Pl-1 core. Pl-1 core and the plagioclase inclusions therein, as well as the plagioclase inclusions in Cpx-1 core, all display the similar An values (supporting information Table S5). In addition, the clinopyroxene inclusions in Pl-1 core also have the similar compositions to Cpx-1 core. All these features suggest that Cpx-1 core and Pl-1 core would probably crystallize from the same melt. The analyzed domains of Cpx-1 core have relatively high Mg# (78.4–80.4), and low Cr (63–847 ppm) and Ni (82–163 ppm) (Figures 5). They are characterized by enrichment of LREE, Rb and Ba but depletion of HFSE, with low REE contents and slightly negative Eu anomalies (supporting information Figure S3). Amphibole inclusions in the Cpx-1 core also have high Mg# of 66.4–67.3, with relatively low REE contents and arc-like trace element distribution patterns (supporting information Figures S3c and S3d). Pl-1 core have low An values of 37.4–42.6, with initial $^{87}Sr/^{86}Sr$ ratios of 0.70749–0.70775 (Figures 6 and 7). All these features suggest that the Cpx-1 core and Pl-1 core were crystallized from a mafic melt that has the arc-like trace element distribution patterns and enriched Sr isotope composition. The high Rb and Ba suggest that the felsic melt in the mantle source would be produced by phengite dehydration-driven partial melting. The negative Eu anomalies in the Cpx-1 core indicate coprecipitation of plagioclase. This is supported by the occurrence of plagioclase inclusions in the Cpx-1 core. The orthopyroxene megacrystals also exhibit negative Eu anomalies and low Cr and Ni contents, suggesting their crystallization in this stage. It is known that partial melting of hydrous peridotite yields a lower Ni mafic melt than that of pyroxenite [*Sobolev et al*., 2005]. Phlogopite is not only an alkali-rich mineral in the lithospheric mantle, but also rich in LILE [*Foley et al*., 1996; *Ionov et al*., 1997]. The mafic melts in this stage are characterized by low Cr and Ni, but high Ba, Rb and K (supporting information Tables S6). This suggests their derivation from partial melting of a

hydrous peridotite with phlogopite breakdown. Such a fertile peridotite clearly results from metasomatism by deeply subducted crust-derived fluid.

The second stage of crystallization is documented by a sudden increase in Cr, Ni, TiO_2 and Al_2O_3 in Cpx-1 mantle and An values in Pl-1 mantle, but decrease in Mg#, Rb and Ba in the Cpx-1 mantle and radiogenic Sr isotope in Pl-1 mantle (Figures 5–7). The Pl-2 core display the similar An values and Sr isotope compositions to those of Pl-1 mantle, suggesting their crystallization in the same stage. The Cpx-1 mantle also exhibits enrichment of LREE but depletion of HREE and HFSE (supporting information Figures S3a and S3b). These suggests their crystallization from an arc-like mafic melt with relatively high Cr, Ni, TiO_2 and Al_2O_3 contents, low Rb, Ba and SiO_2 contents, and low initial $^{87}Sr/^{86}Sr$ ratios. For Cpx-2 megacrystals, they also have high Cr, Ni, TiO_2 and Al_2O_3 but low Rb and Ba, similar to those of the Cpx-1 mantle (supporting information Figures S5a, S5b, and S6). On the chondrite-normalized REE patterns and the primitive mantle-normalized trace element spidergram, they display similar patterns with enrichment of LREE but depletion of HREE and HFSE. The variably low Mg# values and high REE contents probably suggest their crystallization in the relatively late period of this stage. In the second stage, the mafic melts are generally characterized by significantly high Cr, Ni and Al_2O_3 but low Rb and Ba, probably suggesting their derivation from a pyroxenite [*Sobolev et al*., 2005, 2011].

The third stage of crystallization occurs in the outer rims of Cpx-1, Amp-2, Pl-1 rim, Pl-2 rim and minerals in matrix. Cpx-1 rim and Cpx in matrix all have significantly lower contents of Cr, Ni, TiO_2 and Al_2O_3 than Cpx-1 mantle and Cpx-2 (supporting information Figures S5a, S5b, and S6). They also display low Mg# values and high SiO_2 contents. For trace elements, they have the highest REE contents and obviously negative Eu anomalies with arc-like distribution patterns. Amp-2 and Amp in matrix also have similar features with high REE contents but low Mg#, TiO_2 and Al_2O_3 contents, which are significantly different from those of Amp-1 in the Cpx-1 core (supporting information Figures S5c and S5d). Pl-1 rim, Pl-2 rim and plagioclases in the matrix also have the same element and isotope features, different from those of Pl-1 mantle and Pl-2 core that crystallized in stage two (Figures 6 and 7; supporting information Table S5). All these observations suggest that these minerals were crystallized in the last stage of magmatic evolution.

The compositions of melts in equilibrium with crusyallized minerals can be estimated by using appropriate mineral-melt partition coefficients. By doing this, we can see more directly how the magma composition could be changed during the three stages of mineral crystallization. The magma Mg# values in the first stage (Melt 1) were estimated to be 49–53 (Ave. = 51; supporting information Table S7) based on the Mg# values of Cpx-1 core, using a clinopyroxene-melt partition coefficient $K_D(Fe/Mg)^{mineral/melt} = 0.27$ [*Putirka*, 1999*; Putirka et al*., 2003]. And the magma Mg# values in the second (Melt 2) and third (Melt 2) stage were estimated to be 48–50 (Ave. = 49) and 45–47(Ave. = 46) based on the Mg# values of Cpx-1 mantle and rim, respectively. The trace element composition of melts in equilibrium with the Cpx-1 also has been calculated by applying $D_{Cpx/melt}$ values experimentally determined for basaltic systems [*Adam and Green*, 2006, supporting information Table S7]. The average incompatible element composition of melts in equilibrium with the Cpx-1 core (Melt 1) is characterized by enrichment of LILE (especially Rb and Ba), positive Pb anomalies but depletion of HFSE (Nb, Ta and Ti) on the primitive mantle-normalized trace element spidergram (Figure 9). The melts in equilibrium with the Cpx-1 mantle (Melt 2) and Cpx-1 rim (Melt 3) exhibit different distribution patterns, which have significantly low Rb and Ba contents (Figure 9 and supporting information Figures S7a and S7b). Similar to the Cpx-1 mineral zoning, Cr and Ni contents also increase from Melt 1 to Melt 2, then decrease rapidly in Melt 3 (supporting information Figures S7c and S7d). Therefore, the calculated melt compositions of Melt 1 to Melt 3 directly record the magma composition changed during the three stages of magma evolution.

Pressures for the three stages of mineral crystallization are also estimated based on the compositions of clinopyroxene using the geobarometer of *Nimis* [1999]. Since the mafic magmas were derived from partial melting the enriched mantle sources that were metasomatized by continental crust-derived felsic melt, zircon would be probably saturated early in the melt during mafic magmatism. A crystallization temperature of 900±50°C can be estimated by using the Ti-in-zircon geothermometer of *Ferry and Watson* [2007]. Assuming the crystallization temperature of clinopyroxene is also 900°C,

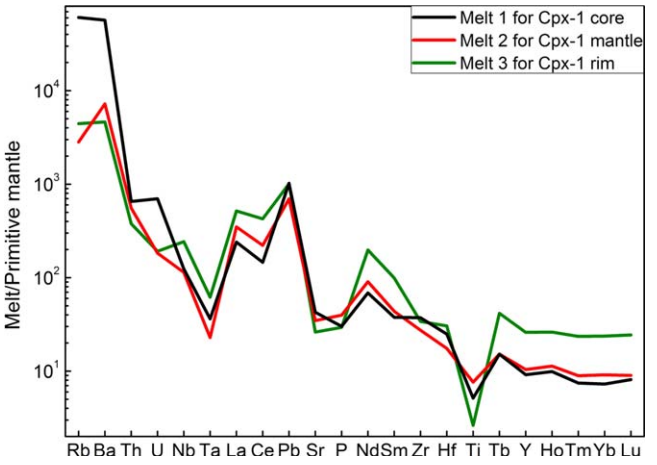

Figure 9. Primitive mantle-normalized trace element spidergrams of the average melt compositions in equilibrium with Cpx-1 calculated by clinopyroxene-melt partition coefficient $D_{Cpx/melt}$ [*Adam and Green*, 2006]. The primitive mantle trace element values are after *McDonough and Sun* [1995]

the estimated pressures for the crystallization of Cpx in the first and second stages are ~800 MPa. The crystallization pressures of Cpx-1 rim and Cpx in matrix (the third stage) are ~600 MPa, significantly lower than those in the first and second stages. The underestimated T by 20°C could propagate into a 100 MPa increase in calculated P for Cpx [*Nimis*, 1999], thus it is difficult to quantify the pressure accurately. Nevertheless, the crystallization pressure in the third stage is significantly lower than that in the first and second stages. As such, magma ascent and differentiation would have occurred mainly in the process from the second to third stages. Therefore, the compositional zonings of minerals record the variations in melt composition from early to late, which can be best accounted for by the magma mixing through accumulation of different batches of mafic melts with possible magma recharge in the level of continental crust.

Magma mixing is a common process during mafic magmatism. The resulted magmas exhibit transitional properties between different bathes of magmas, commonly having the following geochemical features [e.g., *Poli et al.*, 1996; *Maclennan et al.*, 2003; *Maclennan*, 2008; *Davidson et al.*, 2007; *Sun et al.*, 2010]: (1) heterogeneous whole-rock element and isotope compositions; (2) variable element and isotope compositions in single mineral crystals (from core to rim) or between different mineral crystals such as zircon, Cpx, Amp and Pl; (3) variable compositions of mineral inclusions in early crystallized phases. Different $^{87}Sr/^{86}Sr$ ratios also occur across Pl phenocrysts and between Pl phenocrysts and groundmass in MORB [*Lange et al.*, 2012], demonstrating the magma mixing of mafic melts derived from partial melting of the heterogeneous asthenospheric mantle. Major and trace element zonations of Cpx and Pl phenocrysts were reported in Icelandic basalts [*Winpenny and Maclennan*, 2011], recording the magma mixing between different batches of oceanic basaltic melts. For the Jiaoziyan mafic rocks, they exhibit the variable compositions of whole-rock major-trace elements and radiogenic Nd isotopes, zircon Hf isotopes, Cpx element zoning, and Pl element and isotope zoning. These variations are attributable to the magma mixing between different compositions of mantle-derived mafic melts. The mantle sources of different ultramafic lithologies are responsible for the geochemical variations on the both whole-rock and mineral scales. Therefore, the magma mixing between the different batches of mafic melts would be operated in the level of continental crust during the emplacement of postcollisional mafic magmas in the Early Cretaceous.

6. Petrogenetic Processes in Continental Subduction Factory

It is known that the Dabie-Sulu orogenic belt was built by subduction of the South China Block beneath the North China Block to mantle depths of >120 km [*Zheng*, 2008, 2012], which is demonstrated by the occurrence of coesite and microdiamond in exhumed UHP metamorphic rocks in the orogenic belt [*Okay et al.*, 1989; *Wang et al.*, 1989; *Xu et al.*, 1992]. Partial melting of the deeply subducted continental crust is also evident during the continental collision [*Zheng et al.*, 2011; *Gao et al.*, 2012, 2013; *Chen et al.*, 2013b, 2013c], giving rise to felsic melts with the continental crust-like signatures of trace elements and radiogenic isotopes. Such felsic melts would react with the overlying SCLM wedge peridotite in the Triassic at the slab-mantle interface in the continental subduction channel, generating the fertile and enriched mantle sources for postcollisional mafic magmatism in the Early Cretaceous [*Zheng*, 2012; *Zhao et al.*, 2013].

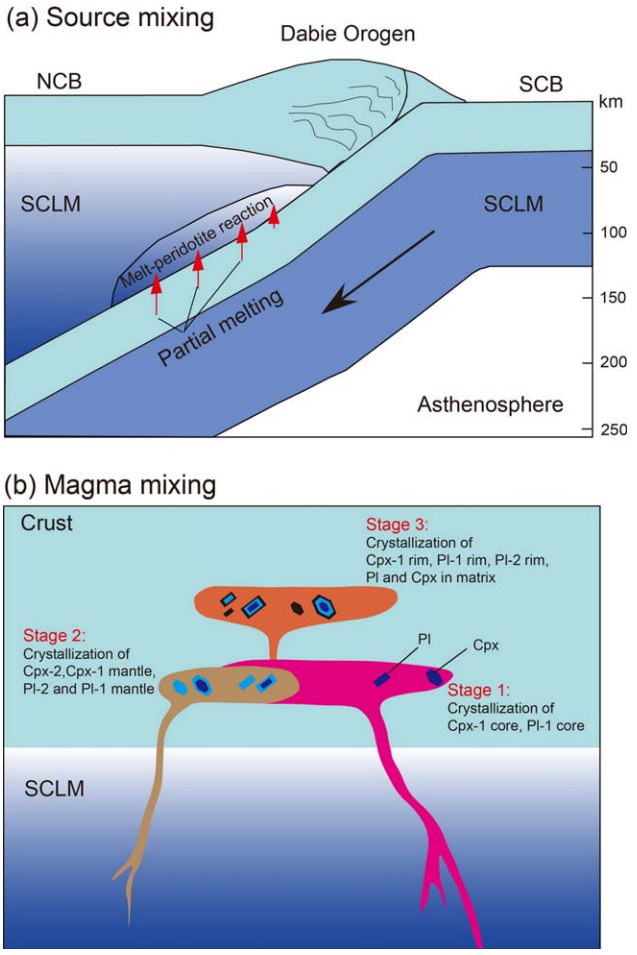

Figure 10. Schematic cartoon illustrating the two stages of mafic magmatism in a continental subduction factory. (a) Source mixing through the melt-peridotite reaction at the slab-mantle interface in continental subduction channel; (b) magma mixing between different batches of mafic melts in postcollisional period. Abbreviations: NCB = North China Block; SCB = South China Block; SCLM = subcontinental lithospheric mantle.

Postcollisional mafic igneous rocks in the Dabie orogen are characterized by arc-like trace element distribution patterns, high initial $^{87}Sr/^{86}Sr$ isotope ratios of 0.7059–0.7113 and negative $\varepsilon_{Nd}(t)$ values of −20.6 to −2.3 [*Chen et al.*, 1998; *Li et al.*, 1998; *Jahn et al.*, 1999; *Wang et al.*, 2005; *Zhao et al.*, 2005, 2011; *Dai et al.*, 2012; *Xu et al.*, 2012] as well as negative $\varepsilon_{Hf}(t)$ values [*Dai et al.*, 2011; *this study*]. These geochemical features indicate the substantial involvement of the continental crust-derived components in their mantle sources. Furthermore, relict zircon cores of Triassic and Neoproterozoic U-Pb ages have been identified in these postcollisional mafic igneous rocks *[Dai et al.*, 2011, 2012; *this study*]. In addition, zircon O isotope analyses yield a large $\delta^{18}O$ variation from 2.3 to 7.3‰, most of which are deviated from the normal mantle $\delta^{18}O$ value of 5.3 ± 0.3‰. And the mafic rocks exhibit the three groups of zircon Hf-O isotope compositions that match the three-layer Hf-O isotope structure for the subducted continental crust in the South China Block [*Dai et al.*, 2011]. These features indicate that different layers of the subducted continental crust were incorporated into the SSZ mantle sources of postcollisional mafic igneous rocks in the Dabie orogen. This led to the source mixing in the Triassic through the melt-peridotite reaction, in which the hydrous felsic melts derived from partial melting of the subducted South China Block react with the overlying SCLM wedge peridotite of the North China Block at the slab-mantle interface in the continental subduction channel [*Dai et al.*, 2012; *Zhao et al.*, 2013]. This generates the metasomatic mantle domains in the orogenic lithospheric mantle, which are referred as the ultramafic metasomes that are susceptible to partial melting relative to the hydrous peridotite [*Zheng*, 2012].

As presented above, the Jiaoziyan mafic rocks are also characterized by arc-like trace element distribution patterns and enriched radiogenic Sr-Nd-Pb isotope features. The relict zircon core of Neoproterozoic U-Pb age has also been identified in these mafic rocks. Therefore, we suggest that the crustal components derived from partial melting of the subducted South China Block were incorporated into the SCLM wedge overlying the slab-mantle interface in the continental subduction channel. The variably negative whole-rock $\varepsilon_{Nd}(t)$ values of −17.6 to −5.2 and zircon $\varepsilon_{Hf}(t)$ values of −29.0 to −7.7 suggest a heterogeneous mantle source, which was generated by the source mixing through reaction of the SCLM peridotite with the different compositions of felsic melts derived from partial melting of the continental crust. In addition, the complex compositional variations of clinopyroxene and plagioclase megacrysts suggest the magma mixing between the different batches of mantle-derived mafic melts. Therefore, the both whole-rock and mineral geochemistries indicate that

at least two kinds of mantle-derived mafic melts were originated from the heterogeneous mantle source due to the source mixing in the Triassic at the slab-mantle interface in the continental subduction channel.

In view of the above observations and interpretations, petrogenesis of the Jiaoziyan mafic igneous rocks can be accounted for by the SARSH model of *Zhao et al*. [2013] in the following five steps. (1) Subduction (S): the continental crust was subducted beneath the SCLM to depths of >120 km. (2) Anatexis (A): anatexis of the subducted continental crust produces the felsic melts that are enriched in LILE and LREE but depleted in HFSE and HREE. (3) Reaction (R): the felsic melts would react with the overlying SCLM wedge peridotite, generating the ultramafic metasomes that are fertile in lithochemistry and enriched in melt-mobile incompatible trace elements and pertinent radiogenic isotopes. (4) Storage (S): the fertile metasomes would be stored in the orogenic lithospheric mantle for tens of million years. (5) Heating (H): the metasomes would become partially melted due to heating at the base of collisional orogen, giving rise to the mafic melts that exhibit the arc-like trace element distribution patterns and variably enriched Sr-Nd-Hf isotope compositions. For the Jiaoziyan mafic igneous rocks, it is the source mixing of Triassic age that results in the petrological and geochemical heterogeneities in the orogenic lithospheric mantle, in which the different compositions of ultramafic metasomes were generated by the reaction between the SCLM wedge peridotite and the felsic melts derived from partial melting of the subducted continental crust (Figure 10a).

Partial melting of the heterogeneous SCLM metasomes in the Early Cretaceous gave rise to the different batches of mafic melts for the magma mixing (Figure 10b). (a) The first batch of mafic melts (Melt 1) has high Rb and Ba but low Cr and Ni contents, and enriched Sr isotopes, which crystallized Cpx-1 core, Pl-1 core and inclusions therein. (b) The second batch of mafic melts (Melt 2) has relatively low Rb and Ba but high Cr and Ni contents, and relatively depleted Sr isotopes, which crystallized Cpx-1 mantle, Cpx-2, Pl-1mantle, and Pl-2 core. The storage and differentiation of mafic melts would result in Cpx-2 with increasing concentrations of incompatible elements. (c) With further mixing between the first and second batches of mafic melts and subsequent differentiation and ascent, the mixed magmas (Melt 3) crystallized Cpx-1 rim, Pl-1 rim, Pl-2 rim, Amp-2 and matrix minerals (Stage 3). Whole-rock initial $^{87}Sr/^{86}Sr$ ratios of gabbro lies between those of Pl-1 core (crystallized from Melt 1) and Pl-1 mantle and Pl-2 core (crystallized from Melt 2), providing isotopic evidence for the magma mixing between Melt 1 and Melt 2 (Figure 7). Pl-1 rim, Pl-2 rim and matrix plagioclase generally have similar initial $^{87}Sr/^{86}Sr$ ratios to those of Pl-2 core, suggesting relatively less contribution of Melt 2 to the generation of gabbro 09JZY11. On the other hand, Pl-1 mantle and Pl-2 core generally have higher An values relative to Pl-1 core, indicate Melt 2 is more mafic than Melt 1. Therefore, the magma mixing in addition to the source mixing is evident in petrogenesis of the Jiaoziyan mafic igneous rocks.

7. Conclusions

Postcollisional mafic igneous rocks from the Jiaoziyan intrusion in the Dabie orogen were emplaced at 126 ± 1 to 130 ± 1 Ma. They contain a relict zircon core of Neoproterozoic U-Pb age, suggesting involvement of the subducted continental crust of the South China Block in their mantle source. They exhibit arc-like trace element distribution patterns and enriched radiogenic Sr-Nd-Hf isotope compositions, suggesting their origination from enriched SCLM metasomes. Furthermore, variable whole-rock and mineral geochemical compositions suggest their origination from a heterogeneous mantle source with different ultramafic lithologies. The Triassic continental collision and crust-mantle interaction in continental subduction channel is suggested as the tectonic mechanism for the generation of fertile and enriched SCLM metasomes. The source mixing is realized by reaction of the overlying SCLM wedge peridotite with the hydrous felsic melts of different compositions derived from partial melting of the subducted continental crust. This melt-peridotite reaction in the Triassic at the slab-mantle interface in the continental subduction channel results in the heterogeneous SCLM metasomes in the orogenic lithospheric mantle. Different batches of mafic melts would be produced by partial melting of these SCLM metasomes in the Early Cretaceous, leading to variable extents of magma mixing (possible recharge) prior to emplacement at the subsurface. Therefore, the both source and magma mixing processes in the continental subduction factory have contributed to the petrogenesis of postcollisional mafic igneous rocks in the continental collision orogen.

Acknowledgments
This study was supported by funds from the Chinese Ministry of Science and Technology (2015CB856102), the Natural Science Foundation of China (41125012, 41221062) and the Fundamental Funds for the Central Universities (WK2080000054). Thanks are due to Zheng Xu, Yi-Xiang Chen and Jilin Zhao for their assistance with field work, Fukun Chen and Jianfeng He for their assistance with radiogenic isotope analyses, to Xiaoming Liu and Honglin Yuan for their assistance with the LA-(MC)-ICP-MS zircon U-Pb and Lu-Hf isotope analyses, to Zhenyu Chen for his assistance with CL imaging, to Ming Feng and Jiangling Xu for their assistance with mineral major elements analyses, to Yongsheng Liu for his assistance with mineral trace elements analyses, and to Yueheng Yang for his assistance with plagioclase in situ Sr isotope analyses. We are grateful to C.-T. A. Lee and an anonymous reviewer for their comments that greatly helped in the improvement of the presentation.

References

Adam, J. and T. Green (2006), Trace element partitioning between mica- and amphibole-bearing garnet lherzolite and hydrous basanitic melt: 1. Experimental results and the investigation of controls on partitioning behaviour, *Contrib. Mineral. Petrol.*, *152*, 1–17.

Barbarin, B. (2005), Mafic magmatic enclaves and mafic rocks associated with some granitoids of the central Sierra Nevada batholith, California: Nature, origin, and relations with the hosts, *Lithos*, *88*, 155–177.

Bebout, G. E. (2007), Metamorphic chemical geodynamics of subduction zones, *Earth Planet. Sci. Lett. 260*, 373–393.

Berly, T. J., J. Hermann, R. J. Arculus, and H. Lapierre (2006), Suprasubduction zone pyroxenites from San Jorge and Santa Isabel (Solomon Islands), *J. Petrol.*, *47*, 1531–1555.

Bonin, B. (2004), Do coeval mafic and felsic magmas in postcollisional to within-plate regimes necessarily imply two constrasting, mantle and crust, sources? A review, *Lithos*, *78*, 1–24.

Bryant, D. L., J. C. Ayers, S. Gao, C. F. Miller, and H. Zhang (2004), Geochemical, age, and isotopic constraints on the location of the Sino-Korean/Yangtze Suture and evolution of the Northern Dabie Complex, east central China, *Geol. Soc. Am. Bull.*, *116*, 698–717.

Carr, M. J., M. D. Feigenson, and E. A. Bennett (1990), Incompatible element and isotopic evidence for tectonic control of source mixing and melt extraction along the Central-American Arc, *Contrib. Mineral. Petrol.*, *105*(4), 369–380.

Chen, B., B.M. Jahn, and C. Wei (2002), Petrogenesis of Mesozoic granitoids in the Dabie UHP complex, Central China: Trace element and Nd-Sr isotope evidence, *Lithos*, *60*, 67–88.

Chen, B., B. M. Jahn, and K. Suzuki (2013a), Petrological and Nd-Sr-Os isotopic constraints on the origin of high-Mg adakitic rocks from the North China Craton: Tectonic implications, *Geology 41*, 91–94.

Chen, D., Y. Wu, Y. Wang, X. Zhi, Q. Xia, and J. Yang (1998), Ages, Nd and Sr isotopic compositions of the Jiaoziyan gabbroic intrusion from the northern Dabie terrain, *Acta Geol. Sin.*, *7*, 29–35.

Chen, L., Z.-F. Zhao, and Y.-F. Zheng (2014), Origin of andesitic rocks: Geochemical constraints from Mesozoic volcanics in the Luzong basin, South China, *Lithos*, *190–191*, 220–239.

Chen, Y.-X., Y.-F. Zheng, and Z. Hu (2013b), Petrological and zircon evidence for anatexis of UHP quartzite during continental collision in the Sulu orogen, *J. Metamorph. Geol.*, *31*, 389–413.

Chen, Y.-X., Y.-F. Zheng, and Z. Hu (2013c), Synexhumation anatexis of ultrahigh-pressure metamorphic rocks: Petrological evidence from granitic gneiss in the Sulu orogen, *Lithos*, *156–159*, 69–96.

Coltorti, M., L. Beccaluva, C. Bonadiman, B. Faccini, T. Ntaflos, and F. Siena (2004), Amphibole genesis via metasomatic reaction with clinopyroxene in mantle xenoliths from Victoria Land, Antarctica, *Lithos*, *75*, 115–139.

Dai, L.-Q., Z.-F. Zhao, Y.-F. Zheng, Q. Li, Y. Yang, and M. Dai M (2011), Zircon Hf-O isotope evidence for crust-mantle interaction during continental deep subduction, *Earth Planet. Sci. Lett.*, *308*, 224–244.

Dai, L.-Q., Z.-F. Zhao, Y.-F. Zheng, and J. Zhang (2012), The nature of orogenic lithospheric mantle: Geochemical constraints from postcollisional mafic-ultramafic rocks in the Dabie orogen, *Chem. Geol.*, *334*, 99–121.

Davidson, J. P., D. J. Morgan, B. L. A. Charlier, R. Harlou, and J. M. Hora (2007), Microsampling and isotopic analysis of igneous rocks: Implications for the study of magmatic systems, *Annu. Rev. Earth Planet. Sci.*, *35*, 273–311.

Fan, W.-M., F. Guo, Y.-J. Wang, and M. Zhang (2004), Late Mesozoic volcanism in the northern Huaiyang tectono-magmatic belt, central China: Partial melts from a lithospheric mantle with subducted continental crust relicts beneath the Dabie orogen?, *Chem. Geol.*, *209*, 27–48.

Foley, S. F., S. E. Jackson, J. D. Fryer, and G. A. J. Greenough (1996), Trace element partition coefficients for clinopyroxene and phlogophite in an alkaline lamprophyre from Newfoundland by LAM-ICP-MS, *Geochim. Cosmochim. Acta*, *60*, 629–638.

Gao, X. Y., Y. F. Zheng, and Y. X. Chen (2012), Dehydration melting of ultrahigh-pressure eclogite in the Dabie orogen: Evidence from multiphase solid inclusions in garnet, *J. Metamorph. Geol.*, *30*, 193–212.

Gao, X. Y., Y. F. Zheng, Y. X. Chen, and Z. Hu (2013), Trace element composition of continentally subducted slab-derived melt: Insight from multiphase solid inclusions in ultrahigh-pressure eclogite in the Dabie orogen, *J. Metamorph. Geol.*, *31*, 453–468.

Guo, F., E. Nakamuru, W. Fan, K. Kobayoshi, and C. Li (2007), Generation of Palaeocene adakitic andesites by magma mixing; Yanji area, NE China, *J. Petrol.*, *48*, 661–692.

Hawkesworth, C. J., J. M. Hergt, R. M. Ellam, and F. McDermott (1991), Element fluxes associated with subduction related magmatism, *Philos. Trans. R. Soc. London A*, *335*, 393–405.

Huang, F., S. G. Li, F. Dong, Q. L. Li, F. Chen, Y. Wang, and W. Yang (2007), Recycling of deeply subducted continental crust in the Dabie Mountains, central China, *Lithos*, *96*, 151–169.

Ionov, D. A., S. Y. O'Reilly, and W. L. Griffin (1997), Volatile-bearing minerals and lithophile trace elements in the upper mantle, *Chem. Geol.*, *141*, 153–184.

Irvine, T. N., and W. R. A. Baragar (1971), A guide to the chemical classification of the common volcanic rocks, *Can. J. Earth Sci.*, *8*, 523–548.

Jahn, B.-m., F.-Y. Wu, C.-H. Lo, and C.-H. Tsai (1999), Crustal-mantle interaction induced by deep subduction of the continental crust: Geochemical and Sr-Nd isotopic evidence from post-collisional mafic-ultramafic intrusions of the northern Dabie complex, central China, *Chem. Geol.*, *157*, 119–146. .

Keay, S., W. J. Collins, and M. T. McCulloch (1997), A three-component Sr-Nd isotopic mixing model for granitoid genesis, Lachlan fold belt, eastern Australia, *Geology*, *25*, 307–310.

Lange, A. E., R. L. Nielsen, F. J. Tepley, and A. J. R. Kent (2012), Diverse Sr isotope signatures preserved in mid-oceanic-ridge basalt plagioclase. *Geology*, *41*, 279–282.

Leake B. E., et al. (1997), Nomenclature of amphiboles: Report of the subcommittee on amphiboles of the international mineralogical association, commission on new minerals and minerals names, *Can. Mineral.*, *35*, 219–246.

Li, S. G., Y. H. Nie, S. R. Hart, and S. G. Zheng (1998), Interaction between subducted continental crust and the mantle II. Sr and Nd isotopic geochemistry of the syncollisional mafic to ultramafic intrusions in northern Dabieshan. *Sci. China (D)*, *28*, 18–22.

Li, S. G., E. Jagoutz, C. H. Lo, Y. Z. Chen, Q. L. Li, and Y. L. Xiao (1999), Sm/Nd, Rb/Sr, and $^{40}Ar/^{39}Ar$ isotopic systematics of the ultrahigh-pressure metamorphic rocks in the Dabie- Sulu belt, central China: A retrospective view, *Inter. Geol. Rev. 41*, 1114–1124.

Liu, Y. C., and S. G. Li (2008), Detachment within subducted continental crust and multi-slice successive exhumation of ultrahigh-pressure metamorphic rocks: Evidence from the Dabie-Sulu orogenic belt, *Chin. Sci. Bull.*, *53*, 3105–3119.

Ma, C. Q., Z. Li, C. Ehlers, K. Yang, and R. Wang (1998), A post-collisional magmatic plumbing system: Mesozoic granitoid plutons from the Dabieshan high-pressure and ultrahigh-pressure metamorphic zone, east-central China, *Lithos*, *45*, 431–456.

Maclennan, J. (2008), Concurrent mixing and cooling of melts under Iceland, *J. Petrol.*, *49*, 1931–1953.

McDonough, W. F., and S.-s. Sun (1995), The composition of the Earth, *Chem. Geol.*, *120*, 223–253.

Maclennan, J., D. McKenzie, K. Gronvold, N. Shimizu, J. Eiler, and N. Kitchen (2003), Melt mixing and crystallization under Theistareykir, northeast Iceland, *Geochem. Geophys. Geosyst.*, *4*(11), 8624, doi:10.1029/2003GC000558.

Middlemost, E. A. K. (1994), Naming materials in magma/igneous rock system, *Earth Sci. Rev.*, *37*, 215–224.

Neave, D. A., E. Passmore, J. Maclennan, G. Fitton, and T. Thordarson (2013), Crystal-melt relationships and the record of deep mixing and crystallization in the AD 1783 Laki eruption, Iceland, *J. Petrol.*, *54*, 1661–1690.

Nimis, P. (1999), Clinopyroxene geobarometry of magmatic rocks: Part 2. Structural geobarometers for basic to acid, tholeiitic and mildly alkaline magmatic systems, *Contrib. Mineral. Petrol.*, *135*, 62–74.

Okay, A. I., S. Xu, and A. M. C. Sengor (1989), Coesite from the Dabie Shan eclogites, central China, *Eur. J. Mineral.*, *1*, 595–598. .

Patiño Douce, A. E., and J. S. Beard (1995), Dehydration-melting of biotite gneiss and quartz amphibolite from 3 to 15 kbar, *J. Petrol.*, *36*, 707–738.

Poli, G., S. Tommasini, and A. N. Halliday (1996), Trace elements and isotopic exchange during acid-basic magma interaction processes, *Trans. R. Soc. Edinburgh Earth Sci.*, *87*, 225–232.

Prouteau, G., B. Scaillet, M. Pichavant, and R. Maury (2001), Evidence for mantle metasomatism by hydrous silicic melts derived from subducted oceanic crust, *Nature*, *410*, 197–200.

Putirka, K. D. (1999), Clinopyroxene + liquid equilibria to 100 kbar and 2450 K, *Contrib. Mineral. Petrol.*, *135*, 151–163.

Putirka, K. D., H. Mikaelian, F. Ryerson, and H. Shaw (2003), New clinopyroxene-liquid thermobarometers for mafic, evolved, and volatile-bearing lava compositions, with applications to lavas from Tibet and the Snake River Plain, Idaho. American, *Mineralogist*, *88*, 1542–1554.

Rapp, R. P., and E. B. Watson (1995), Dehydration melting of metabasalt at 8–32 kbar: Implications for continental growth and crust-mantle recycling, *J. Petrol.*, *36*, 891–931.

Rapp, R. P., N. Shimizu, M. D. Norman, and G. S. Applegate (1999), Reaction between slab-derived melts and peridotite in the mantle wedge: Experimental constraints at 3.8 GPa, *Chem. Geol.*, *160*, 335–356.

Rapp, R. P., Norman, M. D., D. Laporte, G. M. Yaxley, H. Martin, and S. F. Foley (2010), Continent formation in the Archean and chemical evolution of the cratonic lithosphere: Melt-rock reaction experiments at 3–4 GPa and petrogenesis of Archean Mg-diorites (sanukitoids), *J. Petrol.*, *51*, 1237–1266.

Ringwood, A. E. (1990), Slab-mantle interactions: 3. Petrogenesis of intraplate magmas and structure of the upper mantle, *Chem. Geol.*, *82*, 187–207.

Sobolev, A. V., A. W. Hofmann, S. V. Sobolev, and I. K. Nikogosian (2005), An olivine-free mantle source of Hawaiian shield basalts, *Nature*, *434*, 590–597.

Sobolev, S. V., A. V. Sobolev, D. V. Kuzmin, N. A. Krivolutskaya, A. G. Petrunin, N. T. Arndt, V. A. Radko, and Y. R. Vasiliev (2011), Linking mantle plumes, large igneous provinces and environmental catastrophes, *Nature*, *477*, 312–316.

Spandler, C., and C. Pirard (2013), Element recycling from subducting slabs to arc crust: A review, *Lithos*, *170–171*, 208–223.

Stern, R. J. (2002), Subduction zones, *Rev. Geophys.*, *40*(4), 1012, doi:10.1029/2001RG000108.

Sun, J.-F., J.-H. Yang, F.-Y. Wu, X.-H. Li, Y.-H. Yang, L.-W. Xie, and S. A. Wilde (2010), Magma mixing controlling the origin of the Early Cretaceous Fangshan granitic pluton, North China Craton: In situ U-Pb age and Sr-, Nd-, Hf- and O-isotope evidence, *Lithos*, *120*, 421–438.

Sun, S.-s., and W. F. McDonough (1989), Chemical and isotopic systematics of oceanic basalts: Implications for mantle composition and processes, *Geol. Soc. Spec. Publ.*, 42, 313–345.

Tang, J., Y.-F. Zheng, Y.-B. Wu, B. Gong, X. P. Zha, and X.-M. Liu (2008a), Zircon U-Pb age and geochemical constraints on the tectonic affinity of the Jiaodong terrane in the Sulu orogen, China, *Precambrian Res.*, *161*, 389–418.

Tang, J., Y.-F. Zheng, B. Gong, Y.-B. Wu, T.-S. Gao, H.-L. Yuan, and F.-Y. Wu (2008b), Extreme oxygen isotope signature of meteoric water in magmatic zircon from metagranite in the Sulu orogen, China: Implications for Neoproterozoic rift magmatism, *Geochim. Cosmochim. Acta*, *72*, 3139–3169.

Tatsumi, Y., and S. Eggins (1995), *Subduction Zone Magmatism*, 211 pp., Blackwell Sci., Oxford, U. K.

Tiepolo, M., and R. Tribuzio (2008), Petrology and U-Pb zircon geochronology of amphibole-rich cumulates with sanukitic affinity from Husky Ridge (Northern Victoria Land, Antarctica): Insights into the role of amphibole in the petrogenesis of subduction-related magmas, *J. Petrol.*, *49*, 937–970.

Wang, X.-M., J.-G. Liou, and H.-K. Mao (1989), Coesite-bearing eclogites from the Dabie Mountains in central China, *Geology*, *17*, 1085–1088.

Wang, Y.-J., W.-M. Fan, T. Peng, H. Zhang, and F. Guo (2005), Nature of the Mesozoic lithospheric mantle and tectonic decoupling beneath the Dabie Orogen, Central China: Evidence from Ar/Ar geochronology, elemental and Sr-Nd-Pb isotopic compositions of early Cretaceous mafic igneous rocks, *Chem. Geol.*, *220*, 165–189.

Willbold, M., and A. Stracke (2010), Formation of enriched mantle components by recycling of upper and lower continental crust, *Chem. Geol.*, *276*, 188–197.

Winpenny, B., and J. Maclennan (2011), A partial record of mixing of mantle melts preserved in Icelandic phenocrysts, *J. Petrol.*, *52*, 1791–1812.

Xu, H. J., C. Q. Ma, Y. R. Song, J. F. Zhang, and K.Ye (2012), Early Cretaceous intermediate-mafic dykes in the Dabie orogen, eastern China: Petrogenesis and implications for crust–mantle interaction, *Lithos*, *154*, 83–99.

Xu, S. T., W. Su, Y. C. Liu, L. L. Jiang, S. Y. Ji, A. I. Okay, and A. M. C. Sengor (1992), Diamonds from the Dabie Shan metamorphic rocks and its implication for tectonic setting, *Science*, *256*, 80–82.

Yang, J.-H., F.-Y. Wu, S. A. Wilde, L.-W. Xie, Y.-H. Yang, and X.-M. Liu (2007), Tracing magma mixing in granite genesis: In situ U-Pb dating and Hf-isotope analysis of zircons. *Contrib. Mineral. Petrol.*, *153*, 177–190.

Yaxley, G. M., and D. H. Green (1998), Reactions between eclogite and peridotite: Mantle refertilisation by subduction of oceanic crust, *Schweiz. Mineral. Petrogr. Mitt.*, *78*, 243–255.

Zhang, C., C. Ma, F. Holtz, J. Koepke, P. E. Wolff, and Berndt J. (2013), Mineralogical and geochemical constraints on contribution of magma mixing and fractional crystallization to high-Mg adakite-like diorites in eastern Dabie orogen, East China, *Lithos*, *172–173*, 118–138.

Zhang, H. F., S. Gao, Z. Zhong, B. Zhang, L. Zhang, and S. Hu (2002), Geochemical and Sr-Nd-Pb isotopic compositions of Cretaceous granitoids: Constraints on tectonic framework and crustal structure of the Dabieshan ultrahigh-pressure metamorphic belt, China, *Chem. Geol.*, *186*, 281–299.

Zhao, Z.-F., and Y.-F. Zheng (2009), Remelting of subducted continental lithosphere: Petrogenesis of Mesozoic magmatic rocks in the Dabie-Sulu orogenic belt, *Sci. China, Ser. D*, *52*, 1295–1318.

Zhao, Z.-F., Y.-F. Zheng, C.-S. Wei, Y.-B. Wu, F. Chen, and B.-m. Jahn (2005), Zircon U-Pb age, element and C-O isotope geochemistry of post-collisional mafic-ultramafic rocks from the Dabie orogen in east-central China, *Lithos*, *83*, 1–28.

Zhao, Z.-F., Y.-F. Zheng, C.-S. Wei, and Y.-B. Wu (2007), Post-collisional granitoids from the Dabie orogen in China: Zircon U-Pb age, element and O isotope evidence for recycling of subducted continental crust, *Lithos*, *93*, 248–272.
Zhao, Z.-F., Y.-F. Zheng, C. S. Wei, F. K. Chen, X. M. Liu, and F.-Y. Wu (2008), Zircon U-Pb ages, Hf and O isotopes constrain the crustal architecture of the ultrahigh-pressure Dabie orogen in China, *Chem. Geol.*, *253*, 222–242.
Zhao, Z.-F., Y.-F. Zheng, C.-S. Wei, and F.-Y. Wu (2011), Origin of postcollisional magmatic rocks in the Dabie orogen: Implications for crust-mantle interaction and crustal architecture, *Lithos*, *126*, 99–114.
Zhao, Z.-F., L.-Q. Dai, and Y.-F. Zheng (2013), Postcollisional mafic igneous rocks record crust-mantle interaction during continental deep subduction, *Sci. Rep.*, *3*, 3413; doi:10.1038/srep03413.
Zheng, Y.-F. (2008), A perspective view on ultrahigh-pressure metamorphism and continental collision in the Dabie-Sulu orogenic belt, *Chin. Sci. Bull.*, *53*, 3081–3104.
Zheng, Y.-F. (2012), Metamorphic chemical geodynamics in continental subduction zones, *Chem. Geol.*, *328*, 5–48.
Zheng, Y.-F., and J. Hermann (2014), Geochemistry of continental subduction-zone fluids, *Earth Planets Space*, *66*, 93.
Zheng, Y.-F., B. Fu, B. Gong, and L. Li (2003), Stable isotope geochemistry of ultrahigh pressure metamorphic rocks from the Dabie-Sulu orogen in China: Implications for geodynamics and fluid regime, *Earth Sci. Rev.*, *62*, 105–161.
Zheng, Y.-F., Y.-B. Wu, F.-K. Chen, B. Gong, L. Li, and Z.-F. Zhao (2004), Zircon U-Pb and oxygen isotope evidence for a large-scale ^{18}O depletion event in igneous rocks during the Neoproterozoic, *Geochim. Cosmochim. Acta*, *68*, 4145–4165.
Zheng, Y.-F., J.-B. Zhou, Y.-B. Wu, and Z. Xie (2005), Low-grade metamorphic rocks in the Dabie-Sulu orogenic belt: A passive-margin accretionary wedge deformed during continent subduction, *Inter. Geol. Rev.* ,*47*, 851–871.
Zheng, Y.-F., R.-X. Chen, and Z.-F. Zhao (2009), Chemical geodynamics of continental subduction-zone metamorphism: Insight from studies of the Chinese Scientific Drilling (CCSD) core samples, *Tectonophysics*, *475*, 327–358.
Zheng, Y.-F., Q.-X. Xia, R.-X. Chen, and X.-Y. Gao (2011), Partial melting, fluid supercriticality and element mobility in ultrahigh-pressure metamorphic rocks during continental collision, *Earth Sci. Rev.*, *107*, 342–374.
Zheng, Y.-F., W.-J. Xiao, and G.-C. Zhao (2013a), Introduction to tectonics of China, *Gondwana Res.*, *23*, 1189–1206.
Zheng, Y.-F., Z.-F. Zhao, and Y.-X. Chen (2013b), Continental subduction channel processes: Plate interface interaction during continental collision, *Chin. Sci. Bull.*, *58*, 4371–4377.